Final Technical Report

THE DETECTION OF ULF-ELF EMISSIONS FROM MOVING SHIPS

March 1977

Electrical Geophysics Laboratory

Sponsored By

Defense Advanced Research Projects Agency
ARPA Order No. 2600

The views and conclusions contained in this document are those of the authors and should not be interpreted as necessarily representing the official policies, either expressed or implied, of the Defense Advanced Research Projects Agency or the U. S. Government.

Electrical Engineering Research Laboratory
The University of Texas at Austin
Austin, Texas 78712

THE DETECTION OF ULF-ELF EMISSIONS FROM MOVING SHIPS

by

F.X. Bostick, Jr., H.W. Smith and J.E. Boehl

Contractor: The University of Texas at Austin

Contract Number: DAAH01-74-C-0345

Effective Date of Contract: December 4, 1973

Contract Expiration Date: September 4, 1974

Amount of Contract: $ 17,500

ARPA Order Number. 2600

Principal Investigators: Dr. F. X. Bostick, Jr.
Phone: (512) 471-1174

Dr. H. W. Smith
Phone: (512) 471-3101

This research was supported by the Defense Advanced Research Projects Agency of the Department of Defense and was monitored by the U. S. Army Missile Command under Contract Number DAAH01-74-C-0345.

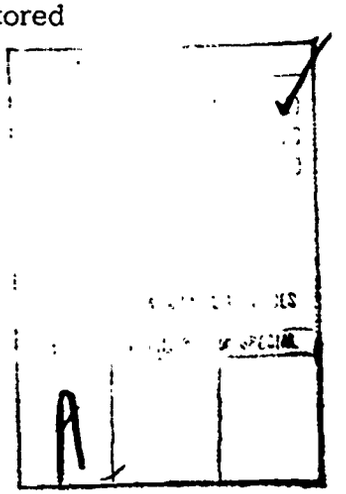

TABLE OF CONTENTS

SUMMARY

The Electrical Geophysics Laboratory of The University of Texas performed a series of measurements of the electromagnetic emissions from merchant ships passing through the Corpus Christi Ship Channel near Port Aransas, Texas. Analysis of the recorded signals shows that they correspond closely to the fields excited by a horizontal electric dipole source moving with the ship. Also recorded were the levels of the natural electromagnetic background. Using these levels the maximum ranges at which a matched filter could extract the ship emission signals are derived. For conditions typical of the open ocean detection ranges of up to 2 km are obtained. Also considered are the effect of electromagnetic noises generated by ocean surface waves moving the conductive sea water in the presence of the geomagnetic field.

I. INTRODUCTION

During the months of September and October of 1973, the Electrical Geophysics Laboratory of The University of Texas operated sensitive electric and magnetic field recording equipment at a shore site adjacent to the Corpus Christi Ship Channel near Port Aransas, Texas. The purpose of the experiment was to record the electric and magnetic field emissions from passing merchant ships in the frequency range extending from approximately 10^{-2} Hz to 5 Hz. In addition, measurements were made of the background noises that would serve to limit the minimum levels at which the emissions could be identified. From these measurements maximum ranges at which the ships could be detected by sensing their electromagnetic emissions have been computed.

One additional consideration was included in the range computations. This involves the theoretical computation of the electromagnetic noises that would be generated by ocean waves moving conductive sea water in the presence of the geomagnetic field. This was done in anticipation of the fact that an actual detection station may be situated at sea. At a sea site the wave noises would add to the natural background noises to further limit the maximum range of detection. An appendix presenting the theoretical derivation of the wave noise fields has been included with this report.

II. THE MEASUREMENTS

A. General

The location of the field site adjacent to the Corpus Christi Ship Channel is shown in Figure 1. Figure 2 shows a plan view of the field site layout including the sensor positions and the ship channel margins.

During the period September 18 through October 7, a total of 55 data runs were recorded. Of this total 37 involved the measurement of the electromagnetic emissions of passing ships, 13 involved recordings of the background noise levels when no ships were in the vicinity of the sensors, 4 were calibration runs and 1 involved the recording of parallel electric field sensing lines to test the noise levels of the electrodes. All of these runs are summarized in Table 1. The runs made during ship passages are designated with the name of the ship. The other runs are designated as to type.

Each data run whether made for the purpose of sensing the emissions from a passing ship or to determine the level of natural background activity, consisted of recording the data in two forms. One was a strip chart record of the analog signals. The other was a digital tape recording of the data sampled and digitized at 0.1 second intervals. The digital tapes contain ten minutes of data giving a total of 6,000 points per run for each component signal recorded.

During ship runs the ships were tracked by visual sightings made with a surveyor's transit. The location of the transit is indicated in Figure 2. The time of visual passage of the ship's bow or stern, depending upon whether the slant range was closing or opening respectively, was recorded at angles of 30° and 60° either side of a 0° or perpendicular sighting on the channel. The times of both bow and stern passages were recorded at the 0° position.

B. Equipment

The equipment used to record both the electromagnetic ship emissions and the background noises consisted of apparatus to sense both the electric and magnetic fields. This apparatus was designed and built by the Electrical Geophysics Laboratory and has been used to record low level fluctuations in the geomagnetic field (geomagnetic micropulsations) and the associated electric fields resulting from the induced earth currents (telluric currents) in a variety of applications.

Each of two orthogonal electric field components tangent to the earth's surface is sensed indirectly by measuring the potential difference between earthed electrodes implanted at each end of a baseline. The potential difference, V, measured between the two electrodes is related to the electric field by the expression

$$V = \int_P \bar{E} \cdot \overline{d\ell}$$

where the path P follows the wires connecting the two electrodes to the potential sensing apparatus. The potential sensing equipment consists of differential input amplifiers in cascade with a network of post amplifiers and filters, the purpose of the latter being to amplify and condition the measured potential difference for digitization and storage.

Each of three orthogonal components of the magnetic field are sensed with one of three induction magnetometers that are constructed by winding a coil of copper wire around a mumetal bar. The high magnetic permeability of the mumetal serves to concentrate the flux in the windings and increase the sensitivity of the induction sensor. The aspect ratio of the bar has been designed so that its demagnetization factor desensitizes the sensor to variations in the permeability of the mumetal caused by various influencing environmental factors. An absolute calibration accuracy of 2% has consistently been observed for these induction magnetometers.

The voltages induced in the magnetic field sensors are amplified in solid state chopper type preamplifiers. These amplifiers have been specially designed to provide very low noise amplification of the induced signals at the impedance levels presented by the sensors.

Post amplification and filtering is similar to that used in the electric field system.

III. DATA PRESENTATION AND ANALYSIS

A. General

Of the total of 37 runs made during ship passages, the 10 exhibiting the highest quality data were selected for analysis. The quality of the data were measured by the absence of extraneous cultural noises or irregularities caused by equipment malfunctions. No judgement was made on the basis of the size or character of the emission signals. As may be seen in the data presentation to follow some of the ships produced large emission signals while for others almost none were detected. One of the most persistent sources of extraneous noise was the presence of moving automobiles in the vicinity of the sensors during a ship passage. The field site was located in an area of free public access and it was considered impossible to stop all vehicular traffic during a data run.

Of the 13 data runs made on the background noise levels 10 were considered of high enough quality to receive further analysis. The results of only 4 of the 10 background runs analyzed are presented here. It was felt that this number was adequate to characterize the different type of noise fields observed.

B. Physical Ship Parameters

The transit sightings made during ship passages were analyzed to yield the ship parameters length, velocity and acceleration. For the analysis, it was assumed that each ship followed a course lying along the center line of the channel. The position, x_b, of the bow of the ship relative to its position, x_o, at the time of the first 60° sighting with closing range is assumed to be given by

$$x_b = x_o + vt + \frac{a}{2} t^2$$

The position, x_s, of the stern with respect to the position x_o is expressed by

$$x_s = x_o - L + vt + \frac{a}{2} t^2$$

The parameters x_o, v (velocity at t=0), a (acceleration) and L (ship's length) were then determined by solving for those values that produce a minimum mean square best fit to the observed position data. The parameters thus determined for each of the 10 ships for which data were analyzed are presented in Table 2. The standard deviation of the estimated length parameter, L, is also indicated to provide a measure of the scatter in the data. Also included in the tabulations of Table 2 is the direction of the ships course.

C. Spectral Analysis

The first step in the spectral analysis of the recorded data consisted of Fourier transforming the sampled time series for each electromagnetic field component. A Fast Fourier Transform routine was used and this required that each series contain a number of sample points equal to an even power of 2. Since each data run produced series that contained 6,000 points a decision had to be made whether to expand each series to 8,192 points by the addition of zeros or to truncate the 6,000 available points to 4,096. The second alternative was adopted because it was reasoned that the dominant spectral components would be generated when the ship was closest to the sensors and this period of time was relatively short compared to the total length of time required for the entire 10 minute data run.

The power density spectra computed from the Fourier transforms of the component fields recorded during the 10 ship passages and 3 background runs selected for presentation are shown in Figures 16 through 28. These spectra have been smoothed to reduce the number of points necessary for visual presentation. The smoothing filter has an approximately constant percentage bandwidth of 26 percent.

D. Strip Chart Recordings

Reproductions of the original strip charts for the 10 selected ship passages and 3 background noise runs are shown in Figures 3 through 16. Each chart includes a coded time signal for temporal reference. In the case of a ship passage, the slant range from the midpoint of the sensor to the ship's stern is indicated for each component signal. The sensitivity of each trace is also indicated on the chart. The units of measure are those commonly used in geophysics. The electric field intensity, E, is measured in millivolts per kilometer (mv/km) and the magnetic flux density, B, is measured in gamma (γ) where $1\gamma = 10^{-9}$ Webers per square meter.

As was pointed out in Section IIB, the electric field was sensed indirectly by measuring the potential difference between two separated electrodes. It is this potential difference that is actually recorded on the strip charts. The indicated E field units have been obtained simply by dividing the measured potential difference by the straight line distance between the sensing electrodes. This is an accurate representation of the electric field only if that field is uniform over the span of the array and if there is negligible extraneous voltage induced in the electrode wires. This extraneously induced voltage is caused by the time rate of change of magnetic flux linking the loop

formed by the straight line path between the electrodes and the actual path of the wires connected to the electrodes. For the slow rate of changes of the magnetic field encountered at the low frequencies involved in this study, this induced voltage is negligible for the wire layouts actually used.

It should be pointed out that the signals recorded on the strip charts have been filtered in an attempt to condition (prewhiten) on the average the signals for digitization. The sensitivities indicated on the charts pertain only to the midband regions of these filters. In some instances, the character of the signals outside this passband has been rather severely modified.

E. Analysis of Electromagnetic Emissions

Reference to the strip chart reproductions in Figures 3, 4 and 10 shows that the emissions from the three ships, Stainless Trader, Benja River and Mariotte are particularly strong and that most of the component signals can be distinguished from the noise to slant ranges in excess of 3,000 ft. Because these signals are so clear it was decided to compare their envelope functions with those that would be produced by a horizontal electric dipole source following the same course as the ship. Such a source is chosen for comparison since it is assumed that the recorded emissions are excited by the ship's propeller modulating the corrosion currents flowing in dipolar fashion between different parts of

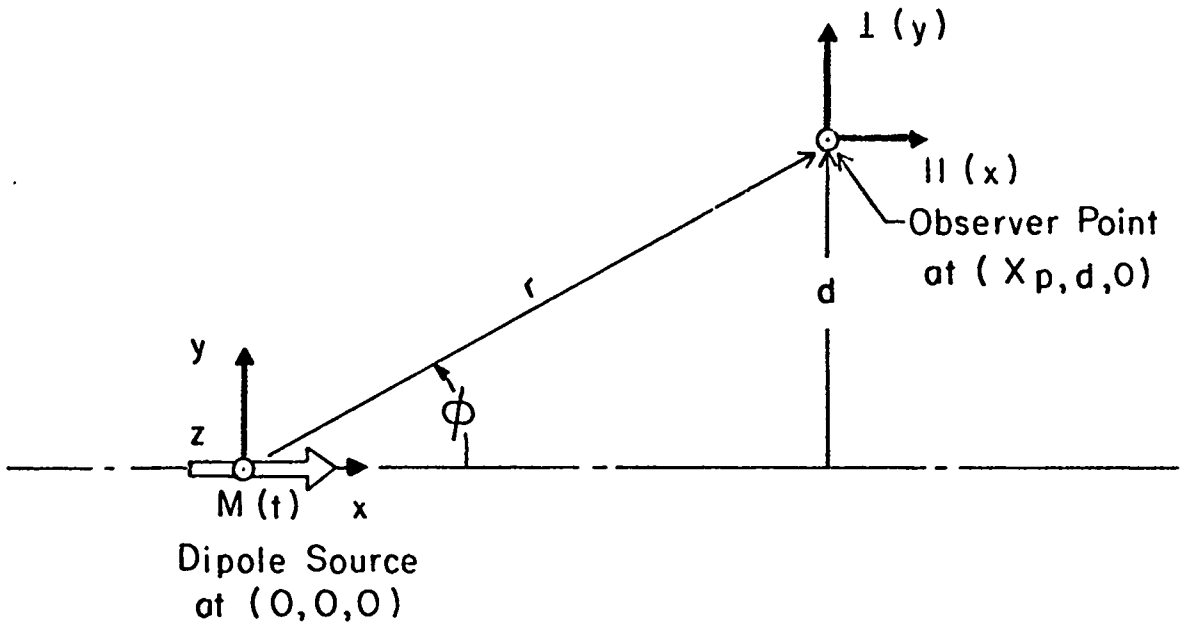

Figure III-1

the ship. In computing the signals generated by the dipole source it is assumed that the dipole is situated at the water's surface at the position of the ship's stern and that it is oriented parallel to the keel. These assumptions represent approximations but the errors that they cause should not seriously affect the principal features of comparison of the computed and measured signals.

As shown in Figure III-1, the dipole of moment M follows a straight line path. The earth is assumed to be uniformly conducting with conductivity, σ, and magnetic permeability, μ_o, equal to that of

free space. The dipole provides a quasi sinusoidal time signal with radian angular fundamental frequency ω_o. At the point of closest approach, it passes a distance d from an observer point where the fields are computed. A rectangular Cartesian coordinate system with axes x, y and z is positioned at the dipole source so that the x axis points in the direction of motion. The positive z direction is up. The coordinate system is assumed to move with the source with the dipole moment pointing in the positive x direction.

Simulating the measurements, the field components are computed in axes parallel ($\|$) and perpendicular ($\perp$) to the dipole path. As may be seen in Figure III-1, the $\|$ and $\perp$ axes are parallel to the x and y axes, respectively.

Formulas for the field components at the observer point are derived from expressions presented by Bannister, [Bannister, 1966]. The derived equations are

$$E_{\|} = \frac{M}{2\pi\sigma r^3}\left[(3\cos^2\phi - 2) + (1+\gamma r)\,e^{-\gamma r}\right] \qquad (1)$$

$$E_{\perp} = \frac{M}{2\pi\sigma r^3}\sin\phi\cos\phi \qquad (2)$$

$$B_{\|} = \frac{\mu_o M}{2\pi r^2}\left[4I_1K_1 - \frac{\gamma r}{2}(I_oK_1 - I_1K_o)\right]\sin\phi\cos\phi \qquad (3)$$

$$B_{\perp} = \frac{\mu_o M}{2\pi r^2}\left[(4\sin^2\phi - 1)\, I_1 K_1 - \frac{\gamma r}{2}\,(I_o K_1 - I_1 K_o)\sin^2\phi\right] \tag{4}$$

and

$$B_{v} = \frac{M}{2\pi\gamma^2 r^2}\left[3 - (3 + 3\gamma r + \gamma^2 r^2)\, e^{-\gamma r}\right]\sin\phi \tag{5}$$

where

$$\gamma = \sqrt{j\omega_o \mu_o \sigma} \tag{6}$$

and I_o, I_1, K_o and K_1 are modified Bessel Functions with argument $\gamma r/2$. Equations (1) through (5) actually represent the envelope functions of the computed signals and must be multiplied by a sinusoidal time factor to simulate the recorded quasi-sinusoidal time traces.

The computed dipole fields are compared to the measured emission signals by comparing the magnitudes of the normalized envelope functions. The envelope functions for the data are scaled from the strip chart records and are normalized by dividing by the peak value during passage. The envelopes of the computed signals are also normalized by the peak value attained as the dipole moves past the observer point.

The magnitudes of the normalized envelope functions measured from the three ships Stainless Trader, Benja River and Mariotte, are compared with the same functions computed for the moving dipole

source in Figures 29, 30 and 31, respectively. The experimental data are plotted as individual points. The theoretical curves are displayed with a solid line.

The fundamental frequency of the recorded quasi-sinusoidal signals was somewhat different for each of the three ships and also varied to some extent with time as each ship passed by. The interval over which the frequency varied extended from 1.2 Hz to 2 Hz. For the computed signals a value of 1.5 Hz was used. A value of one mho per meter was used for the conductivity, σ. This is somewhat smaller than the conductivity of the sea water but is probably near the value of the very porous sediments both underlying and adjacent to the ship channel.

The agreement between the measured and computed data is seen to be excellent. The small differences could easily be caused by the ships following a course slightly to one side or the other of the ship channel or by the small differences in the fundamental frequency of the emission signals. In the opinion of the authors, this close agreement between theory and experiment provides clear evidence that the signals behave like those of a classical horizontal electric dipole.

IV. OCEAN WAVE NOISE ANALYSIS

A. Electromagnetic Noise due to Ocean Waves

Equations for the electric and magnetic fields generated by ocean waves in the conductive sea water have been derived using simple Airy surface wave theory. The derivation is presented in Appendix A. The Airy theory deals with a wave for which the water surface varies sinusoidally with both time and space. If such a wave arbitrarily propagates in the + x horizontal direction and the water motions within the wave are independent of the horizontal y direction, then the water's surface, η, is expressed by

$$\eta(x,t) = \underline{a}e^{j(\omega t - kx)} \tag{7}$$

where $\underline{a}$ is the peak amplitude of the surface undulation: The symbol t represents time and

$$k = \frac{2\pi}{\lambda}$$

is the propagation constant associated with the wave where the wavelength is λ. For this study the water is assumed to be deep enough to allow the "deep water approximation" to be used to derive the dispersion relation

$$k = \frac{\omega^2}{g} \tag{8}$$

where g is the acceleration due to gravity.

The subsequent derivation of the electromagnetic fields induced by the wave motions perpendicular to the geomagnetic field, $\overline{B}_o$, separates the induced fields into two parts. The sum of these two parts constitutes the whole field generated by the ocean wave. One of the parts has a magnetic field that is transverse to the direction of propagation of the wave and to the water motions within the wave. For the wave of equation (7) this means that the magnetic field has only a y component. It follows that the fields associated with this part are designated Transverse Magnetic (TM). The other part of the fields produced by the wave of equation (7) has only a y component of the electric field. The fields associated with this part are called Transverse Electric (TE). The field equations derived in Appendix A for these fields are:

TM fields:

$$E_x = j\omega \underline{a}\, B_{oy}\, e^{kz} \tag{9}$$

$$E_z = -\omega \underline{a}\, B_{oy}\, e^{kz} \tag{10}$$

$$B_y = 0 \tag{11}$$

TE fields:

$$E_y = -j\omega a(B_{ox} + j\, B_{oz})[e^{kz} - \frac{2k}{k+j\zeta} e^{j\zeta z}] \tag{12}$$

$$B_x = -\underline{a}k\,(B_{ox} + jB_{oz})\left[e^{kz} - \frac{2j\zeta}{(k+j\zeta)}\,e^{j\zeta z}\right] \tag{13}$$

$$B_z = -j\underline{a}k\,(B_{ox} + jB_{oz})\left[e^{kz} - \frac{2k}{(k+j\zeta)}\,e^{j\zeta z}\right] \tag{14}$$

where

$$j\zeta = \sqrt{k^2 + j\omega\mu\sigma} \tag{15}$$

The constant $j\zeta$ is a complex quantity that lies in the first quadrant. The vertical coordinate z is positive upwards. It should be pointed out that the transverse magnetic flux density of equation (11) is zero as a consequence of neglecting displacement currents in favor of the conduction currents in the sea water. This assumption is well justified at the low frequencies involved in this study.

Equations (9) and (10) show that the TM electric field is circularly polarized and is always parallel to a plane of propagation of the water wave. In this case a plane of propagation is any vertical plane containing the direction of propagation of the wave. The subscripts $_{\parallel}$ and $_{\perp}$ are used to denote field components that lie paralle or perpendicular respectively to a plane of propagation. The magnitude of the rotating TM electric field vector is given by

$$E_{\parallel} = \omega\underline{a}\,B_{o\perp}\,e^{kz} \tag{16}$$

The TE electric field described by equation (7) is linearly polarized perpendicular to the plane of propagation. Its magnitude is expressed by

$$E_{\perp} = \omega a B_{o\parallel} \left| e^{kz} - \frac{2k}{k+j\zeta} e^{j\zeta z} \right| \qquad (17)$$

The TE magnetic flux density like the TM electric field is circularly polarized in the plane of propagation and its magnitude is expressed by

$$B_{\parallel} = \underline{a} k B_{o\parallel} \left| e^{kz} - \frac{2j\zeta}{k+j\zeta} e^{j\zeta z} \right| \qquad (18)$$

Equations (16), (17) and (18) form a complete description of the magnitude of the electromagnetic fields generated by an ocean wave having the sinusoidal behavior considered here. Before any attempt is made to evaluate the wave induced fields for typical sea states we must first inject the expressions for the full spectrum of ocean waves that are present in the real ocean.

B. Ocean Wave Spectra

A commonly used [Conference, 1963] expression for the power density spectrum, E(f), of ocean wave heights is

$$E(f) = E(f_o) \left(\frac{f}{f_o}\right)^{-m} e^{-\frac{m}{n}\left[\left(\frac{f}{f_o}\right)^{-n} - 1\right]} . \qquad (19)$$

The parameters m and n control the shape of the density function. The variable f is frequency in Hertz and f_o is the frequency of the mode (maximum) of the density function. $E(f_o)$ is the spectral density at the mode frequency. It should be pointed out here that E(f) refers to the spectral density of peak amplitudes of the ocean waves. The mean square or variance, $\sigma^2(f)$, of the ocean waves is only one half the value of E(f):

$$\sigma^2(f) = \frac{E(f)}{2} \qquad (20)$$

Various investigators have used different values of m and n to match individual sets of experimental data. A sample of the values reported in the literature [Conference, 1963] is shown in Table 3.

Table 3

Investigator	m	n
Neumann	6	2
Burling	5.5	7-9
Roll-Fisher	5	2
Bretschneider	5-9	4

Although the choice is rather arbitrary the values used by Neumann will be used here. These values represent the spectrum for a fully arisen wind driven sea. Substituting $m = 6$ and $n = 2$ into equation (19) gives

$$E(f) = E(f_o)\left(\frac{f}{f_o}\right)^{-b} e^{-3\left[\left(\frac{f}{f_o}\right)^{-2} - 1\right]} \tag{21}$$

The mode frequency for the Neumann spectrum is related to the wind speed, v, through the expression [Defant, 1961]

$$f_o = \frac{g}{2\pi v}\sqrt{\frac{2}{3}} \tag{22}$$

where as indicated previously g is the acceleration due to gravity. The spectral density at the mode frequency is given by

$$E(f_o) = Cf_o^{-6} \tag{23}$$

where

$$C = 1.37 \times 10^{-3} \ (m^2/Hz) \tag{24}$$

gives good agreement with experimental observations.

We may derive the total wave amplitude, E, by integrating the density function to obtain

$$E = \int_0^\infty E(f)\, df. \tag{25}$$

Substituting equation (21) into equation (25) and integrating gives

$$E = f_o \, E_f(f_o) \, K \tag{26}$$

where

$$K = \frac{e^3}{24} \sqrt{\frac{\pi}{3}} = .856 \tag{27}$$

The most important characteristics of the waves can be found in terms of E as [Defant, 1961]

most frequent value	$H_f = 1.414 \sqrt{E}$
average value	$H = 1.772 \sqrt{E}$
significant value	$H_{y_{1/3}} = 2.832 \sqrt{E}$
average of highest 10%	$H_{y_{1/10}} = 3.600 \sqrt{E}$

C. Wave Induced Electromagnetic Noise Spectra

Expressions for the power density spectra of the wave induced noises can now be obtained by combining the wave spectra of Sec V-B with the electromagnetic noise expressions in equations (11), (12) and (13). In so

doing we note that the induced fields have been derived in terms of a sinusoidal water wave with peak amplitude $\underline{a}$. As derived each electromagnetic expression yields the peak value of the indicated field component where that component field varies sinusoidally in response to the water wave. We can compute the power spectral density of the wave induced field components by first squaring each expression and then replacing the square of the wave amplitude, $\underline{a}^2$ by the appropriate spectral density term. For our purposes in this study we choose to compute the spectral density of the mean square or variance of the wave induced fields and this is obtained by letting

$$\underline{a}^2 = \sigma^2(f)$$

Substituting from equation (15) for $\sigma(f)$ obtains

$$\underline{a}^2 = \frac{E}{2} \tag{28}$$

D. Wave Induced Electromagnetic Noise Computations

The expressions for the power density of the wave amplitude and the wave induced noise spectra were programmed for a programmable calculator and the spectrum values computed as a function of frequency for different values of wind speed. Plots of the computed spectra $E(f)$, $P_{E_{\parallel}}$, $P_{E_{\perp}}$ and $P_{B_{\parallel}}$ are shown in Fig. 32 through Fig. 38 respectively. Here the symbol P with a subscript is used to designate the power density spectrum of the field component designated by the subscript. The geophysical units of millivolts per kilometer and gamma have been used for the electric and magnetic fields respectively.

The terms representing the geomagnetic field $B_{o\parallel}$ and $B_{o\perp}$ are each a function of position on the earth's surface as well as the direction of propagation of the water waves. Rather than compute the noise fields for a variety of values for $B_{o\parallel}$ and $B_{o\perp}$ it was decided to use those values that would produce the largest noises and let this constitute a "worst case" value. The largest value for $B_{o\parallel}$ would exist at the geomagnetic poles where

$$B_{o\parallel} = 6 \times 10^{4} \text{ gamma} \tag{29}$$

is typical. The largest value for $B_{o\perp}$ would occur at the magnetic equator for waves propagating magnetically east-west. Typical of this field is the value

$$B_{o\perp} = 3 \times 10^{4} \text{ gamma} \tag{30}$$

The values equations (29) and (30) were used for the computations.

A summary of the equations used to compute the spectra of Figs. 32 through 38 in the units used for the plots is given below.

$$P_{E\parallel} = 10^{-6}\, \omega^2\, \frac{E(f)}{2}\, B_{o\perp}^2\, e^{2kz} \; - \; \frac{(m_y/km)^2}{Hz} \tag{31}$$

$$P_{E\perp} = 10^{-6}\, \omega^2\, \frac{E(f)}{2}\, B_{o\parallel}^2 \left| e^{kz} - \frac{2k}{k+j\zeta} \right|^2 - \frac{(m_y/km)^2}{Hz} \tag{32}$$

$$P_{B\parallel} = k^2\, \frac{E(f)}{2}\, B_{o\parallel}^2 \left| e^{kz} - \frac{2j\zeta}{k+j\zeta}\, e^{j\zeta z} \right|^2 - \frac{\gamma^2}{Hz} \tag{33}$$

$$E(f) = E(f_o)\left(\frac{f}{f_o}\right)^{-6} e^{-3\left[\left(\frac{f}{f_o}\right)^{-2} - 1\right]} - \frac{m^2}{Hz} \tag{34}$$

where:

$$k = \frac{\omega^2}{g} - m^{-1}$$

$$\omega = 2\pi f - \frac{rad}{sec}$$

$$g = 9.81 - \frac{m}{sec}$$

$$j\zeta = \sqrt{k^2 + j\omega\mu_o\sigma} \quad \text{(first quadrant)}$$

$$\mu_o = 4\pi \times 10^{-7} - h_y/m$$

$$\sigma = 4 \text{ mhos/meter}$$

$$B_{o\parallel} = 6 \times 10^4 - \gamma$$

$$B_{o\perp} = 3 \times 10^4 - \gamma$$

$$f_o = \frac{g}{2\pi v}\sqrt{\frac{2}{3}} \quad \text{Hz} \quad \text{(v is wind velocity in m/sec)}$$

$$E(f_o) = 1.37 \times 10^{-3} f_o^{-6} - \frac{m^2}{Hz}$$

V. DETECTION RANGE COMPUTATIONS

The emission signals recorded from passing merchant ships have been shown to agree closely with the fields of a moving horizontal electric dipole. This means that the dipole fields can be used to compute the maximum ranges at which the ship emissions could be detected. For the computations it is assumed that the ranges between the ships and the sensors would be somewhat greater than that which existed at Port Aransas. For larger values of γ, Equations (1) through (6) take the somewhat simpler forms, [Bannister, 1966].

$$E_{\parallel} = \frac{M \cos \omega_o t}{2 \pi \sigma d^3} \left[\left(u^2 - 2\right)\left(u^2 + 1\right)^{-5/2} \right] \tag{35}$$

$$E_{\perp} = \frac{M \cos \omega_o t}{2 \pi \sigma d^3} \left[3u \left(u^2 + 1\right)^{-5/2} \right] \tag{36}$$

$$B_{\parallel} = \frac{\mu_o M \cos \omega_o t}{2 \pi \gamma d^3} \left[3u \left(u^2 + 1\right)^{-5/2} \right] \tag{37}$$

$$B_{\perp} = \frac{\mu_o M \cos \omega_o t}{2 \pi \gamma d^3} \left[\left(2 - u^2\right) \left(u^2 + 1\right)^{-5/2} \right] \tag{38}$$

$$B_v = \frac{\mu_o M \cos \omega_o t}{2 \pi \gamma^2 d^4} \left[\left(u^2 + 1\right)^{-5/2} \right] \tag{39}$$

where

$$u = \frac{x_p}{d} \tag{40}$$

and x_p and d are defined in Figure III-1. The distance variable x_p, measured from the location of the moving dipole to the point of closest approach to the sensors, is assumed to vary with time according to the expression

$$x_p = -vt \tag{41}$$

A cosinusoidal time factor has been included in Equations (35) through (39). The radian angular frequency, $\omega_o = 2\pi f_o$, is the fundamental of the quasisinusoidal emission signals.

For the range computations it is assumed that the component signals are imbedded in background noise. Non-physically realizable matched filters are assumed to be used to extract the signal from the noise. A matched filter has a frequency response that is the complex conjugate of of the Fourier transform of the signal to which it is matched. In order to design the filters necessary to extract the signals of Equations (35) through (39) it is necessary to obtain the Fourier Transforms of those expressions. At this point, it is noted that the component electric field signal $E_{\parallel}$ may be derived from $B_{\perp}$ by multiplying by γ/μ_o. In similar fashion, $E_{\perp}$ may be obtained from $B_{\parallel}$ by multiplying by the same factor. The quantity γ/μ_o is actually $1/\mu_o$ times the wave impedance at the surface of the earth

looking down. It can be shown that for noises originating in sources sufficiently far away, the orthogonal horizontal components of the electric and magnetic fields are related in exactly the same way. This means that the ratio of the signal to the noise is the same for the electric field components as it is for those of the magnetic field. It is redundant to derive the filters and the maximum detection ranges for the components of both fields. For this reason, the calculations are continued only for the three components of the magnetic field.

In order to obtain the Fourier Transforms of Equations (37) through (39) it is noted that each of those expressions may be written in the form

$$B(t) = k\, h(t) \cos \omega_o t \tag{42}$$

where

$$h(t) = f[u(t)] \tag{43}$$

and $f(u)$ is the appropriate function of u in the square brackets. The factor k in (42) includes all of the terms outside the brackets that are constant with respect to u and t. The transform of (42) may be obtained as

$$B(\omega) = \frac{k}{2} \left[H(\omega - \omega_o) + H(\omega + \omega_o) \right] \tag{44}$$

where the transform $H(\omega)$ is most conveniently written in terms of the Fourier Transform of $f(u)$ as

$$H(\omega) = \frac{d}{v} F^*(\lambda). \tag{45}$$

In (45)

$$\lambda = \frac{d}{v} \omega \tag{46}$$

and

$$F(\lambda) = \int_{-\infty}^{\infty} f(u)\, e^{-j\lambda u}\, du \tag{47}$$

is the expression for the Fourier Transform of $f(u)$. The superscript * with F in (45) denotes the complex conjugate.

The three functions of u in the square brackets on the right hand sides of Equations (37) through (39) are designated $f_1(u)$, $f_2(u)$ and $f_3(u)$, respectively. Thus

$$f_1(u) = 3u\,(u^2 + 1)^{-5/2} \tag{48}$$

$$f_2(u) = (2 - u^2)\,(u^2 + 1)^{-5/2} \tag{49}$$

$$f_3(u) = (u^2 + 1)^{-5/2} \tag{50}$$

The Fourier Transforms of (48), (49) and (50) are tabulated, [Bateman, 1954], as

$$F_1(\lambda) = -j\lambda^2 K_1(\lambda) \tag{51}$$

$$F_2(\lambda) = \lambda^2 K_o(\lambda) + \lambda K_1(\lambda) \tag{52}$$

$$F_3(\lambda) = 1/3 \left[\lambda^2 K_o(\lambda) + 2\lambda K_1(\lambda) \right] \tag{53}$$

The functions F_2 and F_3 and the magnitude of F_1 are shown plotted for positive λ in Figure 39. It should be noted that F_2 and F_3 are even functions of λ while F_3 is odd.

In order to complete the Fourier Transforms of the three components of the magnetic field it is necessary to first substitute (51) through (53) into (45). With the aid of (45) the results are substituted into (44). The final result obtained for $B_\perp$ is written as an example of the set of three. The expression is

$$B_\perp(\omega) = \frac{\mu_o M}{4\pi\gamma d^3} \left\{ F_2\left[\frac{d}{v}(\omega - \omega_o)\right] + F_2\left[\frac{d}{v}(\omega + \omega_o)\right] \right\} \tag{54}$$

The frequency response of the filter matched to the $\perp$ component of the magnetic field is the complex conjugate of $B_\perp(\omega)$. Since the expression of (54) is real the equation for the matched filter response is identical to (54).

The response of the filter described by (54) is seen to be the sum of two filter responses. Each has a shape defined by F_2 but one

filter is shifted to the frequency ω_o while the other is shifted to $-\omega_o$. With values for d, v and ω_o typical of the ship detection problem, the response of the filter translated to either one of the two frequencies has negligible amplitude at the other. Thus, the shapes of the matched filters are for all practical purposes the same as those described by the functions F_1, F_2 and F_3. The term

$$\lambda = \frac{d}{v} (\omega \pm \omega_o) \tag{55}$$

represents a normalized frequency variable. For this reason, the curves of Figure 39 can be interpreted as the response of the matched filters on one side of the center frequency and the functions F_1, F_2 and F_3 are referred to as the matched filter shape functions. All of the filters may be described as narrow band pass filters centered on the fundamental frequency of the quasisinusoidal emission signals

The output, $S_F(t)$, of a filter matched to a signal $S(t)$ may be written as

$$S_F(t) = \frac{1}{2\pi} \int_{-\infty}^{\infty} |S(\omega)|^2 e^{-j\omega t} dt \tag{56}$$

It is assumed that this output maximizes at $t = 0$ so that the maximum output of the filter can be written as

$$S_F(0) = \frac{1}{2\pi} \int_{-\infty}^{\infty} |S(\omega)|^2 \, d\omega \tag{57}$$

If the matched filter responds to noise with power density $P_N(\omega)$, the expected value of the rms (standard deviation) of the output, $n_F(t)$, is given by

$$\text{rms} = \tfrac{1}{2}\pi \int_{-\infty}^{\infty} P_N(\omega) |S(\omega)|^2 \, d\omega \tag{58}$$

The detection problem amounts to comparing the character of noise with rms value given by (58) to the maximum output of the filter produced by the signal and expressed by (57).

Two simplifying assumptions are used for the derivations to follow. In the first, the power density $P_N(\omega)$ is assumed to be a relatively slowly varying function of frequency similar to the measured curves shown in Figures 26 through 28. The signal spectrum $S(\omega)$, typical of the component emission signals, has appreciable amplitude only over two very narrow bands of frequencies centered on $\pm \omega_o$. The implication is that $P_N(\omega)$ is essentially constant in the vicinity of the frequencies where $S(\omega)$ has values so that Equation (58) may be written as

$$\text{rms} = \frac{P_N(\omega_o)}{2\pi} \int_{-\infty}^{\infty} |S(\omega)|^2 \, d\omega \tag{59}$$

The remaining calculations are also simplified with the second assumption that the filtered noise is random with a Gaussian amplitude probability distribution.

The maximum range of detection problem is described specifically as follows. The probability with which an independent point of $n_F(t)$ is not to exceed the value of $S_F(0)$ is specified. The maximum range at which this requirement is satisfied is defined to be the maximum range of detection. This range will, of course, be a function of the specified probability.

The probability specification is written as

$$P_r \left| -S_F(0) < n_F(t) < +S_F(0) \right| = P \qquad (60)$$

where P is the specified probability. The specification is chosen to be two sided for the following reason. The filtered signal output is quasisinusoidal, even more so than the unfiltered signal. Although the maximum of the filtered signal theoretically occurs as a positive peak at $t = 0$, in practice the maximum applies to a time interval representing several cycles of the sinusoidal variations. Thus, a filter output that is more negative than $-S_F(0)$ is considered also to be a significant detection. Hence, the probability specification of (60) is written two sided.

Dividing each of the terms inside the braces on the left hand side of (60) by the rms value of the noise gives

$$\Pr\left\{ -C < \frac{n_F(t)}{\text{rms}} < C \right\} = P \tag{61}$$

where

$$C = \frac{S_F(0)}{\text{rms}} \tag{62}$$

The independent sample points of the function $(n_F(t)/\text{rms})$ have zero mean and unit variance so that the values of C for a specified value of P can be obtained from tabulated values of the normal probability integral [Brunk, 1965]. Three different values of C are considered here. They are $P = 0.9$, $P = 0.99$ and $P = 0.999$. The corresponding values of C are subscripted with the complement to P expressed as a percentage.

$$\begin{aligned} C_{10\%} &= 1.645 \\ C_{1\%} &= 2.326 \\ C_{0.1\%} &= 3.291 \end{aligned} \tag{63}$$

The subscript refers to the probability that an independent sample point of $n_F(t)$ will exceed the established detection threshold.

Computation of the maximum detection range for a given value of C begins with Equation (62). Substituting for $S_F(0)$ from (57) and

for rms from (59) and then rearranging gives

$$\left[\frac{1}{2\pi} \int_{-\infty}^{\infty} |S(\omega)|^2 \, d\omega \right]^{\frac{1}{2}} = C_p \, P_N^{\frac{1}{2}} \tag{64}$$

The subscript p indicates the selected value of C.

Equation (64) is now evaluated with the aid of Parseval's theorem written as

$$\frac{1}{2\pi} \int_{-\infty}^{\infty} |S(\omega)|^2 \, d\omega = \int_{-\infty}^{\infty} S^2(t) \, dt \tag{65}$$

The right hand side of (65) is evaluated for $S(t)$ equal to each of the functions $B_{\parallel}$, $B_{\perp}$, and B_v given in Equations (37), (38) and (39). One approximation is used to evaluate the resulting integrals. It is illustrated by writing the integral for the general form of the signal function given in (42).

$$I = \int_{-\infty}^{\infty} K^2 h^2(t) \cos^2 \omega_o t \, dt \tag{66}$$

The envelope function $h(t)$ varies slowly with time compared to the oscillations of $\cos \omega_o t$. In particular it is assumed that $h(t)$ can be considered essentially constant over any one half cycle of the cosine. Thus,

$$I = \int_{t_1}^{t_2} K^2 h^2(t)\, dt \approx K^2 h^2(t_3) \int_{t_1}^{t_2} \cos^2 \omega_o t\, dt \tag{67}$$

where

$$t_1 - t_2 = \frac{\pi}{\omega_o} \tag{68}$$

and the choice of t_3 is immaterial as long as it is between t_1 and t_2. The integral on the right hand side of (67) can be evaluated to give

$$I \approx \frac{K^2 h^2 (t_3)}{2} \tag{69}$$

Since $h(t)$ is assumed almost constant over the interval (t_1, t_2),

$$h^2(t_3)\ (t_2 - t_1) \approx \int_{t_1}^{t_2} h^2 (t)\ dt \tag{70}$$

so that

$$I \approx \frac{K^2}{2} \int_{t_1}^{t_2} h^2 (t)\ dt \tag{71}$$

If the whole t axis is subdivided into consecutive intervals all of which have equal length corresponding to one half cycle of the cosine then

$$I \approx \tfrac{1}{2} \int_{-\infty}^{\infty} K^2 h^2(t)\ dt \tag{72}$$

The substitutions given in (40) and (41) are used with (72) to obtain finally

$$\frac{1}{2\pi} \int_{-\infty}^{\infty} |S(\omega)|^2 \, d\omega \approx \tfrac{1}{2} \frac{d}{v} K^2 \int_{-\infty}^{\infty} f^2(u) \, du \tag{73}$$

The proper forms of K and f from each of Equations (37), (38) and (39) are used in (73) and the resulting integrals evaluated [Dwight, 1960]. The results are substituted into (64) to obtain the three detection equations

1. $B_{\parallel}$

$$d_p = \left(\frac{M}{a_p}\right)^{2/5} \left(\frac{45 \times 10^{-7}}{512 \pi \sigma P_{N_{\parallel}}(\omega_o) f_o v}\right)^{1/5} \tag{74}$$

2. $B_{\perp}$

$$d_p = \left(\frac{M}{a_p}\right)^{2/5} \left(\frac{123 \times 10^{-7}}{512 \pi \sigma P_{N_{\perp}}(\omega_o) f_o v}\right)^{1/5} \tag{75}$$

3. B_v

$$d_p = \left(\frac{M}{a_p 4\pi^2 f_o \sigma}\right)^{2/7} \left(\frac{35 \pi}{256 v P_{N_v}(\omega_o)}\right)^{1/7} \tag{76}$$

It is important to note here that the values of P_N used in (74), (75) and (76) are the two sided power density functions defined for both positive and

negative frequencies. Most power density spectra computed from experimental data including those shown in all of Figures 16 through Figure 28 are one sided and assume that all of the power is in the positive frequencies. It is therefore necessary to divide the one sided power density spectrum values by 2 if those values are to be used in Equations (74), (75) or (76).

It is also important to emphasize the units used for the power density. MKS units are required for Equations (74), (75) and (76). Most experimentalists, however, follow the geophysical convention of using the unit $\gamma = 10^{-9}$ Webers per square meter for the magnetic field and the unit (mv/km) for the electric field. These geophysical units have been used in Figures 16 through 28 so that the appropriate scaling must be done before any values are entered into the detection equations.

A review of the three Equations (74), (75) and (76) shows that B_1 is most likely to give the largest detection range. The only differences between (74) and (75) are the terms in the numerator of the second parenthesis of each equation and the different component noise power densities. In general, there is no reason to expect that the noise power density is different in either axes. This means that the larger numerator factor of (75) causes that equation to yield a larger value for d_p than (74). The power density of the vertical component of the magnetic field noise may, however, be quite a bit smaller than the horizontal components. The extent to which it is smaller depends upon a number of factors including the distribution of

conductivity in the solid earth beneath the sun floor and the depth of the overlying water. In some instances, the small vertical field noises could cause (76) to give a better detection range than (75). However, the vertical field signal falls off more rapidly with range than does either of the horizontal signals so it appears that (75) would in general provide the largest value of d_p.

Assuming this to be the case, Equation (75) is evaluated with the parameters observed for the merchant ships in Port Aransas under two sets of conditions. The first is the set that existed during the Port Aransas measurements. A conductivity of one mho per meter is used for σ and $P_{N_\perp}$ has the value $10^{-5}\ \gamma^2/Hz$. The results are presented in Table 3. The second set of conditions is considered more appropriate to the open ocean. The velocity of each ship is set to 20 knots. The fundamental frequencies of the emissions are scaled from the value measured in Port Arnasas. The scaling assumes that the frequencies are proportional to the velocity of the ship. A conductivity of 5 mhos per meter is used to represent that of the sea water. As before, a noise power density of $10^{-5}\ \gamma^2/Hz$ is used for $P_{N_\perp}$. The resulting d_p values for the different merchant ships are tabulated in Table 4.

The extent to which the noises caused by the surface water waves affect the detection ranges can be determined from the curves of Figures 32 through 38. Consider specifically the case of a magnetic field

measurement made near the surface. The curves of Figure 33 show the power density spectra of magnetic field noises computed for the spectral distribution of wave height energy shown in the curves of Figure 32. The parameter in both plots is wind speed. At frequencies above 1Hz the wave induced magnetic field noise power density is essentially independent of wind speed. The level is below the value of $10^{-5}\ \gamma^2/\text{Hz}$ used for the detection range calculations leading to the results of Tables 3 and 4. This means that the wave induced noises should not materially reduce the maximum detection ranges.

It should be pointed out, however, that a value of $10^{-5}\ \gamma^2/\text{Hz}$ is a typical summertime low latitude value and does not represent a minimum. In some instances, for example, during the winter months in polar regions, the power density of the background noises may be considerably less. In this event, the ocean wave induced noises may indeed serve to limit the maximum detection ranges. The detection range can, however, be increased by measuring the magnetic field at some depth below the water's surface. The effect can be noted with the aid of Figure 36. That figure shows curves of the ocean wave induced magnetic field power density spectra at a depth of 100 meters. The level of power density at frequencies in the 1 to 10 Hz range is seen to be negligible at this depth.

The signals and background noises also attenuate with depth in the sea water but nowhere near as rapidly as the wave induced noises.

A measure of the signal attenuation is obtained by noting that a skin depth at 5 Hz in sea water is roughly 100 meters. This means that at 5 Hz the signal power at 100 meters would be reduced by a factor of about 7. Frequencies below 5 Hz would be attenuated to a lesser extent. It is concluded from the above that for a given set of wave conditions there is some depth of water below which the wave induced noises would have negligible effect on the detection ranges. The limiting factor would be the level of natural background noises.

VI. CONCLUSIONS

This study has been concerned with both the theoretical and experimental aspects of detecting the electromagnetic emissions from ships in motion. Measurements made on merchant ships in the Corpus Christi ship channel clearly indicate that the emission signals behave like the fields of a horizontal electric dipole at the position of the ship.

Based upon this fact, detection ranges are computed for the case where the signals are extracted from the background noises with a matched filter. The ranges obtained depend upon the effective strength of the moment of the source of the emissions. This, of course, varies from ship to ship and may vary with time on a given ship as the condition of the hull and the screws changes. Several of the ships passing through the ship channel produced no measurable emission signals. The assumption

that they could not be detected may not be exactly correct. If the measurements had been processed with a set of matched filters there may have been a low level of emission that could have been detected. However, the maximum detection ranges computed from these ships under typical sea conditions would in any event be less than the smallest range shown in Table 4. Such a range would be too small to be of interest. This would seem to cast some doubt on the efficacy of detection methods based solely on the propeller modulated emissions. They should not be completely discounted, however, because the detection ranges obtained for ships with large source moments have quite reasonable values at around 2 kilometers.

In addition it is noted here that all of the detection range calculations are based on single point measurements of the component fields associated with the emissions. In previous studies [Fowler, 1973], our laboratory has used linear filtering techniques with measurements of the spatial field gradients to significantly reduce the background noise levels. This work was done in connection with studies of the maximum detection ranges that could be achieved by sensing the static dipole moments of moving ships. The frequencies involved were well below those of the present study. Reductions of the noise levels by factors of up to 40 db were produced with filters that corrected for the inhomogeneous distribution of conductivity in the earth. These filters, termed "geology filters", were originally developed at our laboratory.

Similiar techniques could be used to reduce the background noise levels at the frequencies of the propeller emission signals. A reduction of the noise power by a factor of 40 db would increase the detection ranges listed in Tables 3 and 4 by the one fifth power of that factor. This would amount to an increase of 6.3 times and would produce a very usable detection range under sea conditions of over 10 km for the ships with large source moments. The smallest detection range listed in Table 4 would increase to a very respectable value of over 3 km.

With this projected result in mind, the authors recommend that the feasibility of implementing such a system be investigated. On the basis of results of previous studies it is also recommended that such a system incorporate the additional features necessary to detect the static dipole moment. This could be done with the same set of sensors. Simultaneous processing to extract both the static and propeller induced moments should produce a detection system with significant capability.

TABLE 1

SUMMARY OF DATA RUNS

Date	Description of Run	Run No.
09-18	Giovanella d'Amico	091873-1
	Wanderer & David P. Reynolds	091873-2
	Honner	091873-3
	Calibrate	091873-4
09-19	Ero	091973-1
	Melias	091973-2
	Calibrate	091973-3
	Stainless Trader	091973-4
	David P. Reynolds	091973-5
09-21	Benja River	092173-1
	Pitria Star	092173-2
09-24	Background	092473-1
	Background (No Digital Tape)	092473-2
	Chemical Venturer	092473-3
09-25	Background	092573-1
	Background	092573-2
	Calibrate	092573-3
	Inger	092573-4
	Ero	092573-5
	Tumi	092573-6
	Richard	092573-7
	Background	092573-8
09-26	Texas Sun	092673-1
	Background	092673-2
	Background	092673-3
	Richard	092673-4
	Background	092673-5
	David P. Reynolds	092673-6
	Background	092673-7
	Background	092673-8
	Aghios Spyridon	092673-9

TABLE 1
(continued)

Date	Description of Run	Run No.
09-28	Mariotte	092873-1
	Background	092873-2
	Background (No Digital Tape)	092873-3
	Background	092873-4
	Hellenic Ideal	092873-5
09-30	Master Stefanos	093073-1
	Marjorie Lykes	093073-2
	Solholt	093073-3
10-02	La Bonita	100273-1
	Wingull	100273-2
	Gulfcrest	100273-3
	Master Stefanos & Aquacharm	100273-4
10-03	Calibrate	100373-1
	Nopal Tellus	100373-2
	Monmouth	100373-3
10-04	Electrode Test	100473-1
	Hess Trader	100473-2
	David P. Reynolds & Coastal Texas	100473-3
10-05	Richard	100573-1
	Texaco Oregon	100573-2
10-06	Ship (Name Not Recorded)	100673-1
10-07	Rio Balsas	100773-1
	Atlantic Prestige	100773-2
	Nopal Trader	100773-3

TABLE 2

MEASURED SHIP PARAMETERS

Ship	Direction	L (ft.)	σ (ft.)	x_o (ft.)	v (ft./sec.)	a (ft./sec.^{2})
Stainless Trader	Outbound	267	10.9	-4003	28.9	2.10×10^{-2}
Inger	Outbound	659	2.2	-4614	16.2	3.02×10^{-3}
Pitria Star	Outbound	462	1.5	-5324	23.1	1.62×10^{-3}
Benja River	Inbound	437	5.1	-5636	18.2	-6.96×10^{-3}
Texas Sun	Inbound	670	6.8	-5456	14.1	-3.05×10^{-3}
Aghios Spyridon	Inbound	473	4.7	-2405	26.0	-1.03×10^{-3}
Tumi	Inbound	373	14.8	-5372	21.2	2.80×10^{-3}
Mariotte	Outbound	540	8.9	-5274	23.0	5.58×10^{-3}
Gulfcrest	Inbound	618	7.0	-4208	19.4	-8.73×10^{-3}
Nopal Trader	Outbound	429	2.3	-3625	25.5	1.32×10^{-2}

TABLE 3

DETECTION RANGES - MATCHED FILTER

SHIP	M (amp-m)	f_o (Hz)	$d_{10\%}$ (km)	$d_{1\%}$ (km)	$d_{0.1\%}$ (km)
Benja River	119	1.7	3.85	3.35	2.92
Stainless Trader	120	2.0	3.41	2.97	2.58
Nopal Trader	7	1.2	1.24	1.08	.94
Tumi	36	1.2	2.48	2.16	1.88
Gulfcrest	26	1.4	2.15	1.87	1.63
Inger	178	1.4	4.82	4.19	3.65
Texas Sun	53	1.2	3.15	2.74	2.38
Mariotte	179	1.3	4.57	3.98	3.46

TABLE 4

DETECTION RANGES - MATCHED FILTER

SEA CONDITIONS

(σ = 5 v/m, v = 20 Knots, $f_o \sim v$)

SHIP	d 10% (km)	d 1% (km)	d 0.1% (km)
Benja River	2.18	1.90	1.65
Stainless Trader	2.32	2.02	1.76
Nopal Trader	.81	.70	.61
Tumi	1.49	1.30	1.13
Gulfcrest	1.25	1.09	.95
Inger	2.70	2.35	2.04
Texas Sun	1.61	1.40	1.22
Mariotte	2.84	2.47	2.15

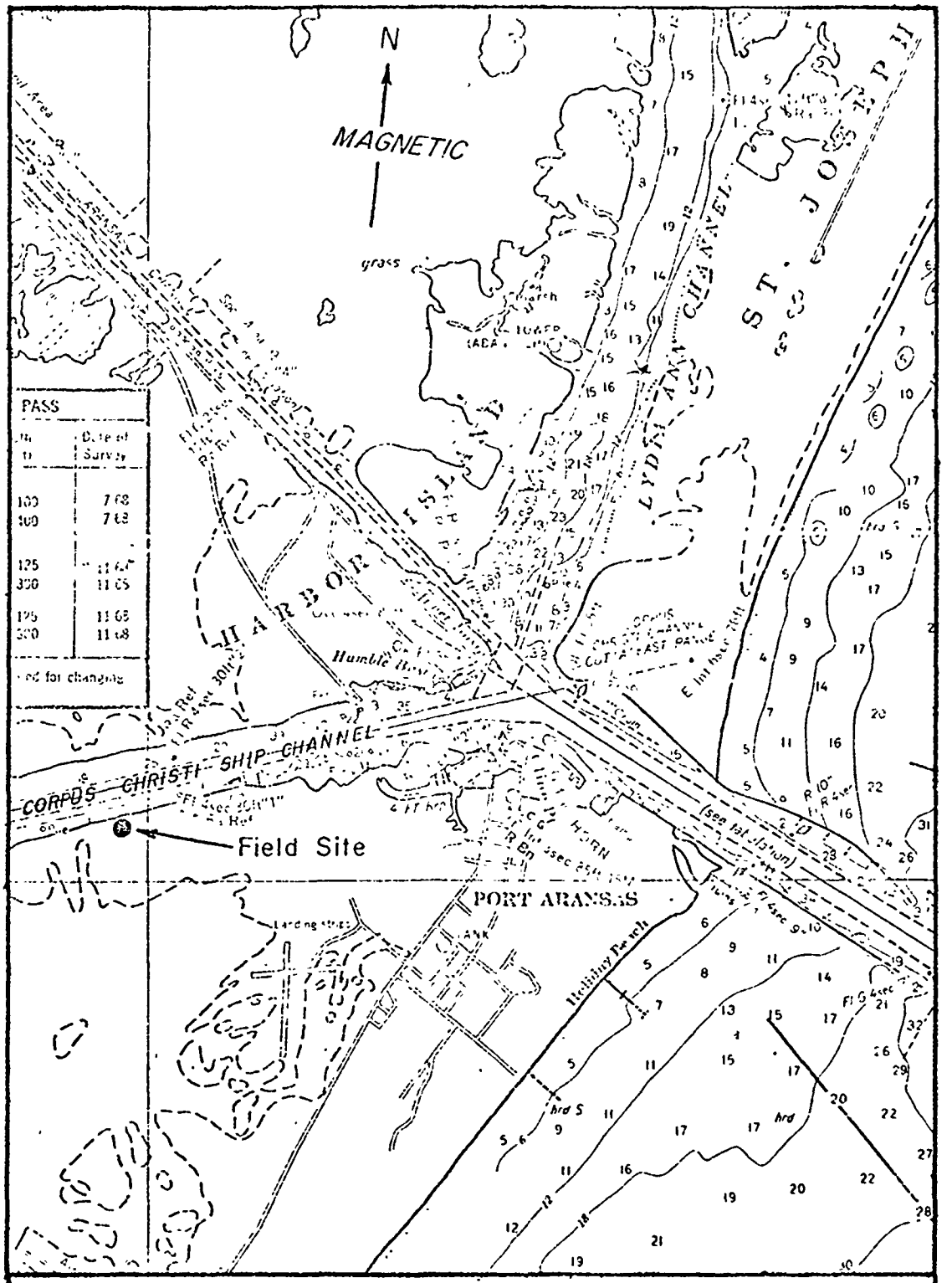

Fig. 1 Field Site Location

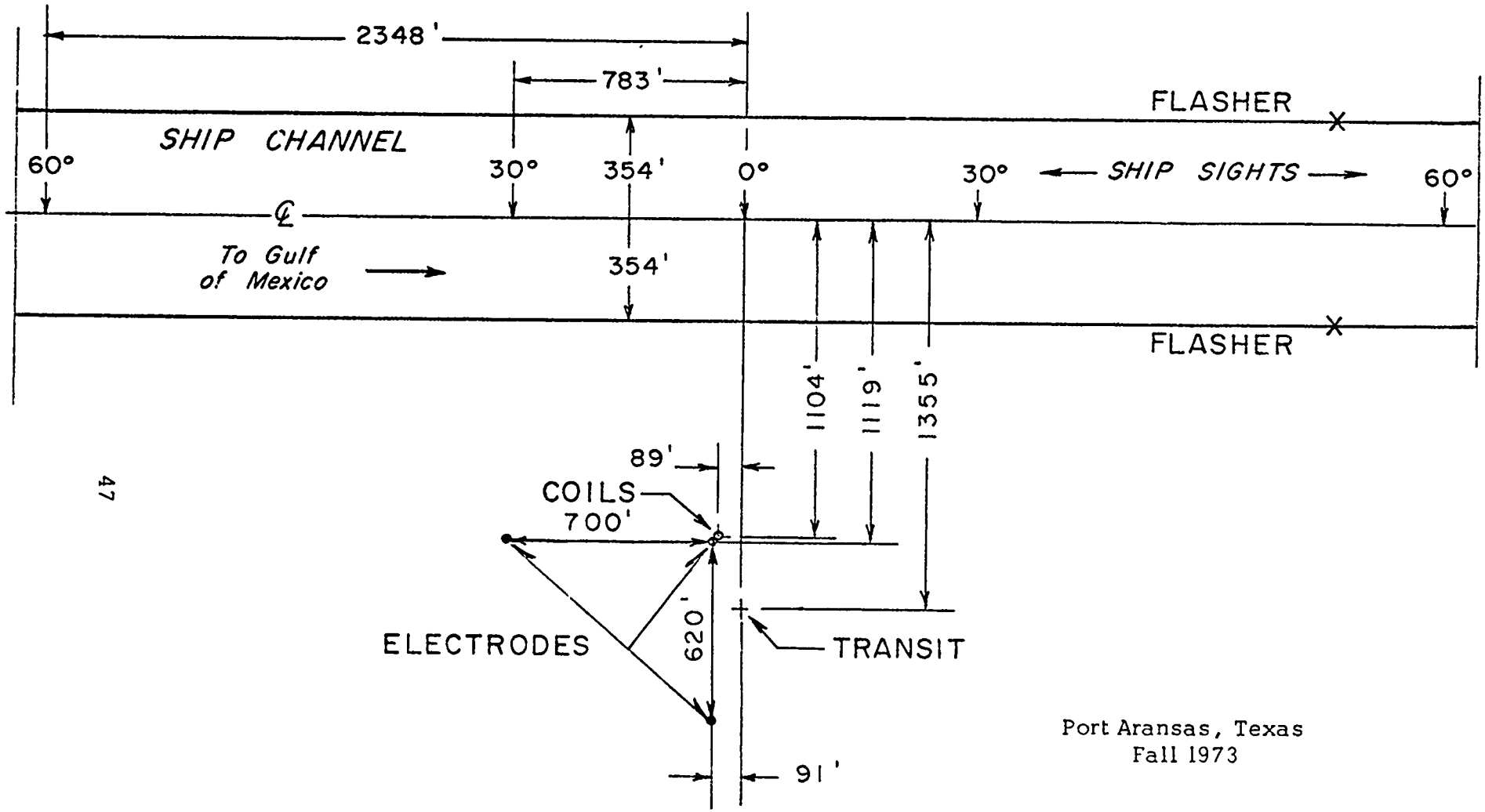

Port Aransas, Texas
Fall 1973

Fig. 2 Measuring Site Layout

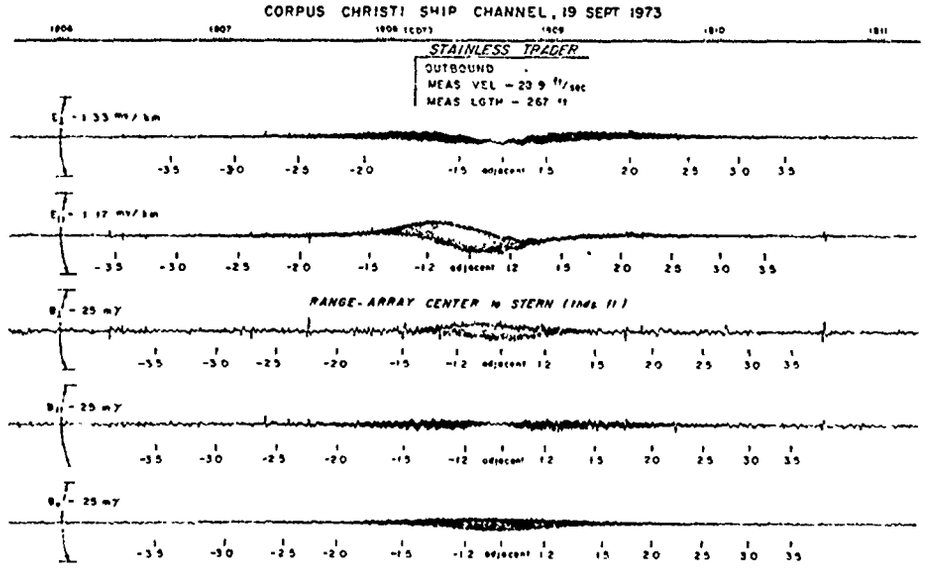

Figure 3. Recorded Time Traces - Stainless Trader

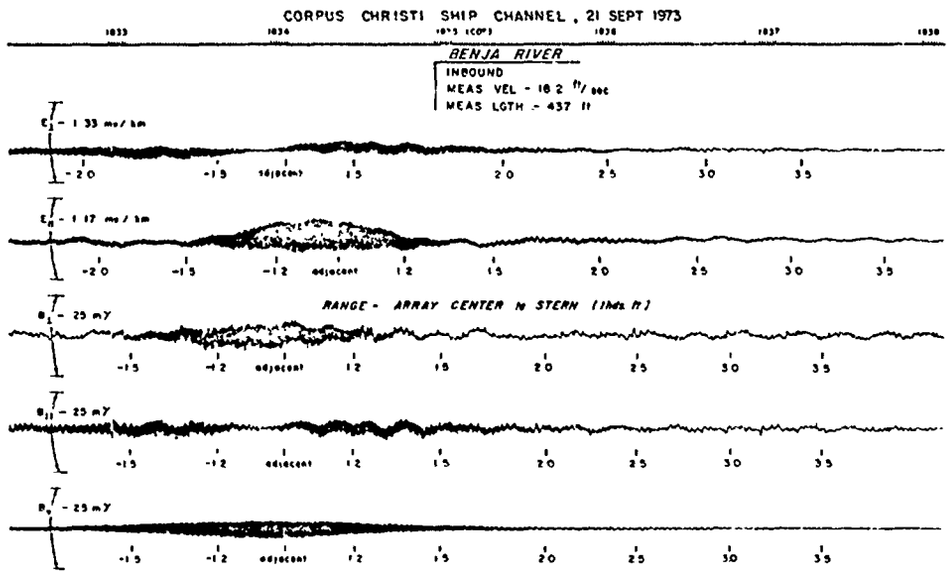

Figure 4. Recorded Time Traces - Benja River

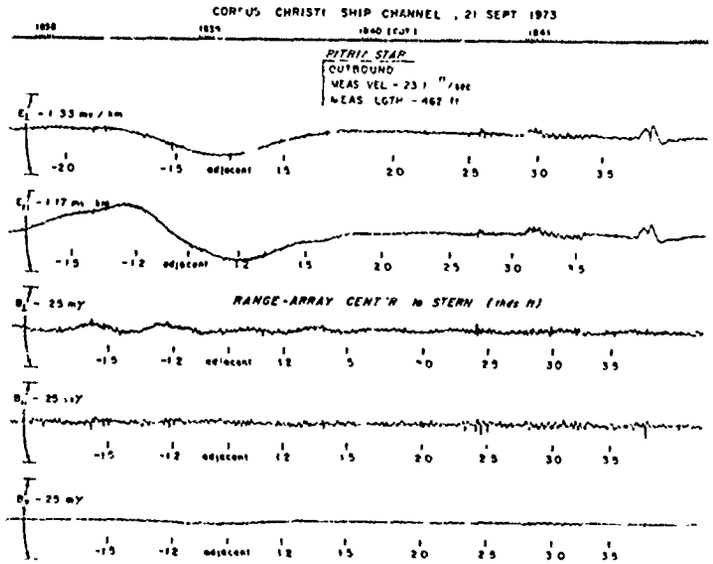

Figure 5. Recorded Time Traces - Pitria Star

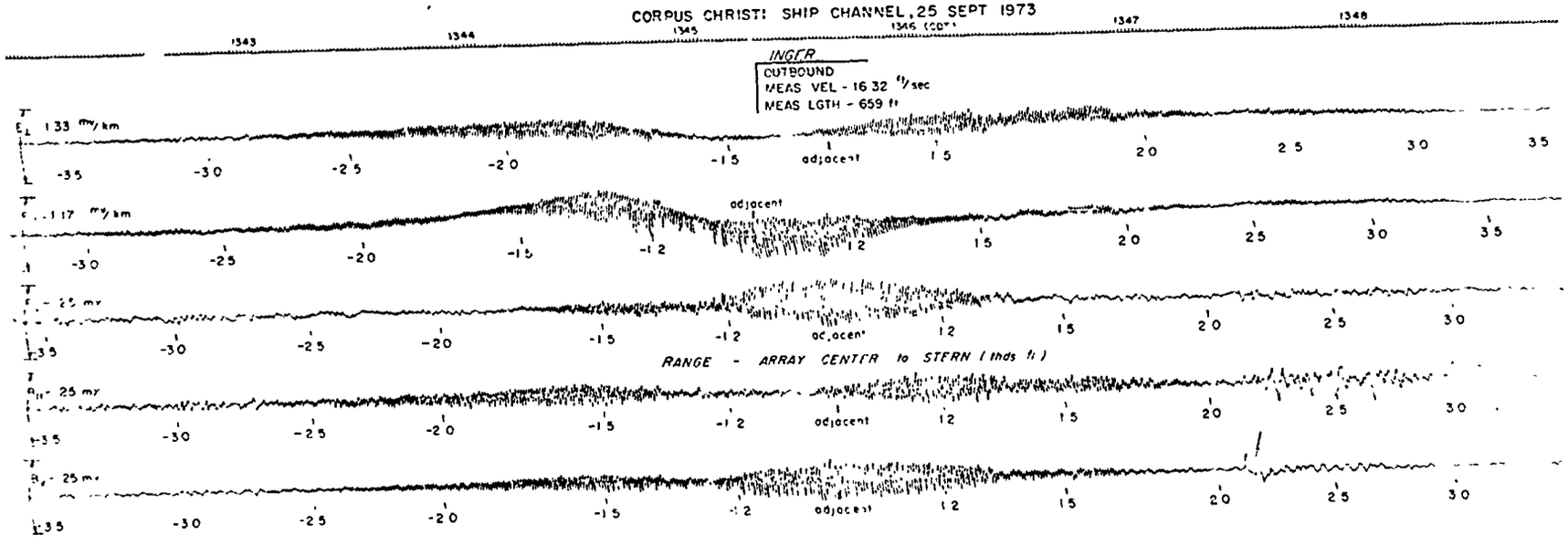

Figure 6. Recorded Time Traces - Inger

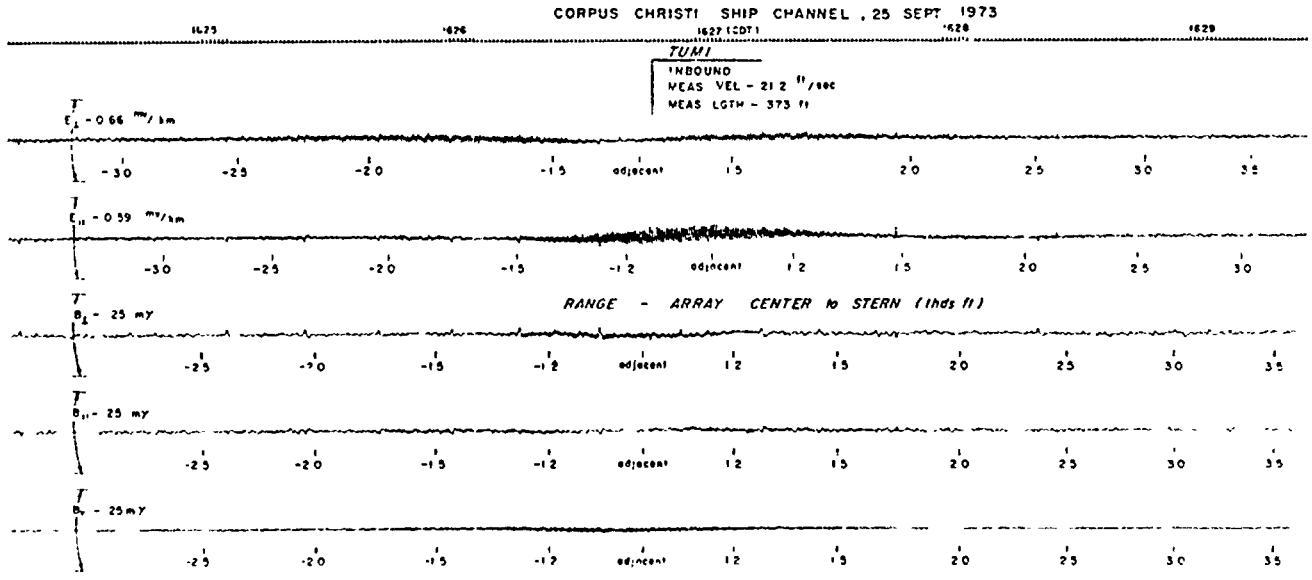

Figure 7. Recorded Time Traces - Tumi

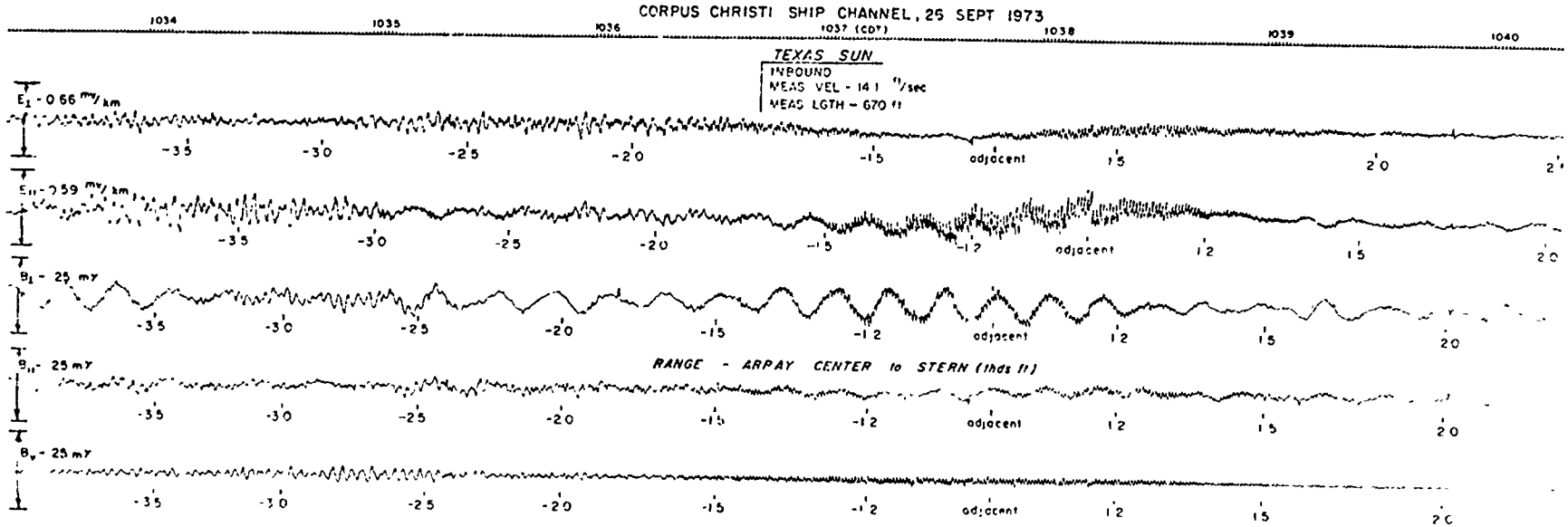

Figure 8. Recorded Time Traces - Texas Sun

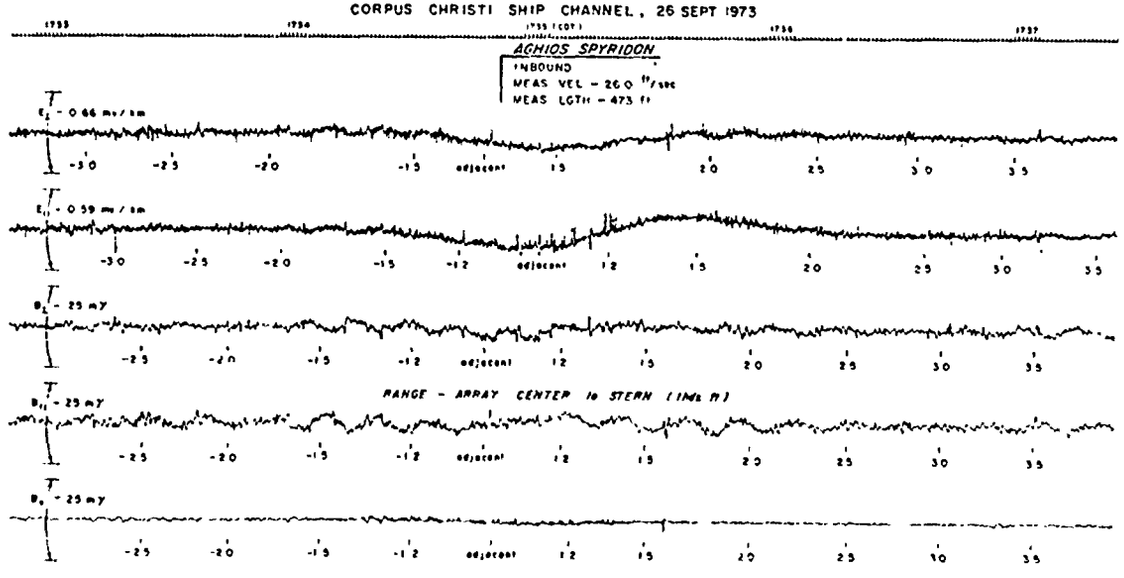

Figure 9. Recorded Time Traces - Aghios Spyridon

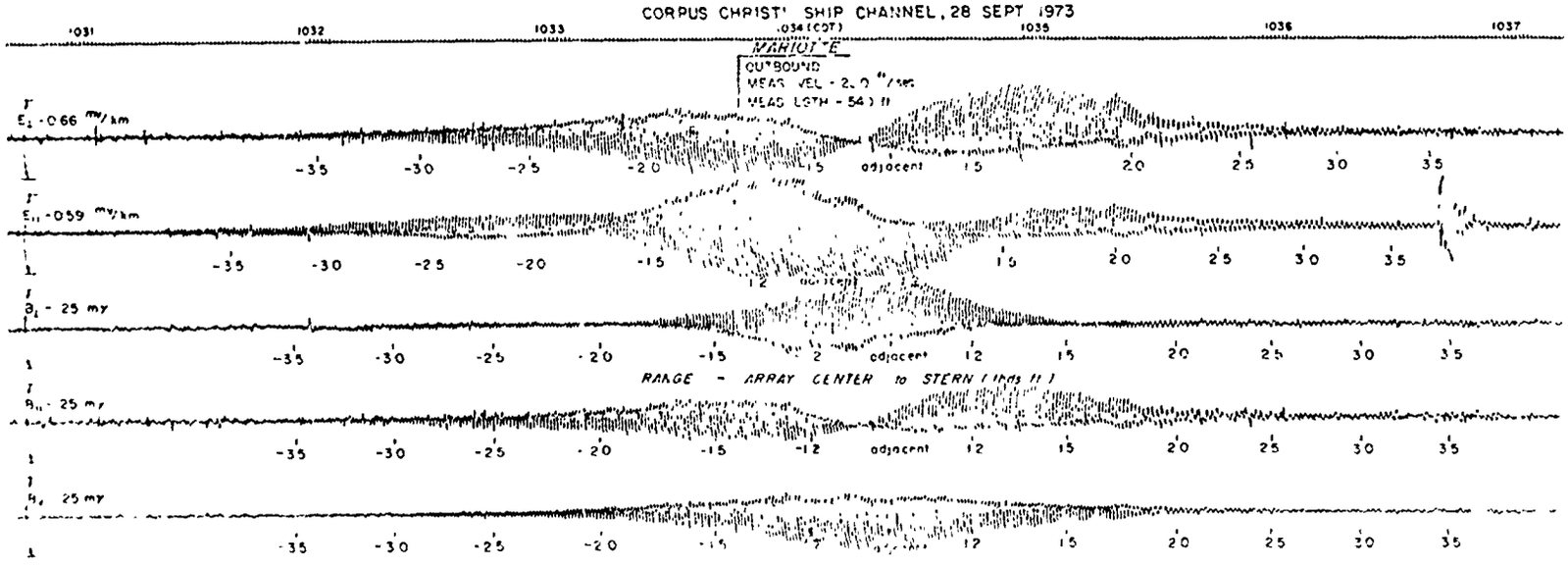

Figure 10. Recorded Time Traces - Mariotte

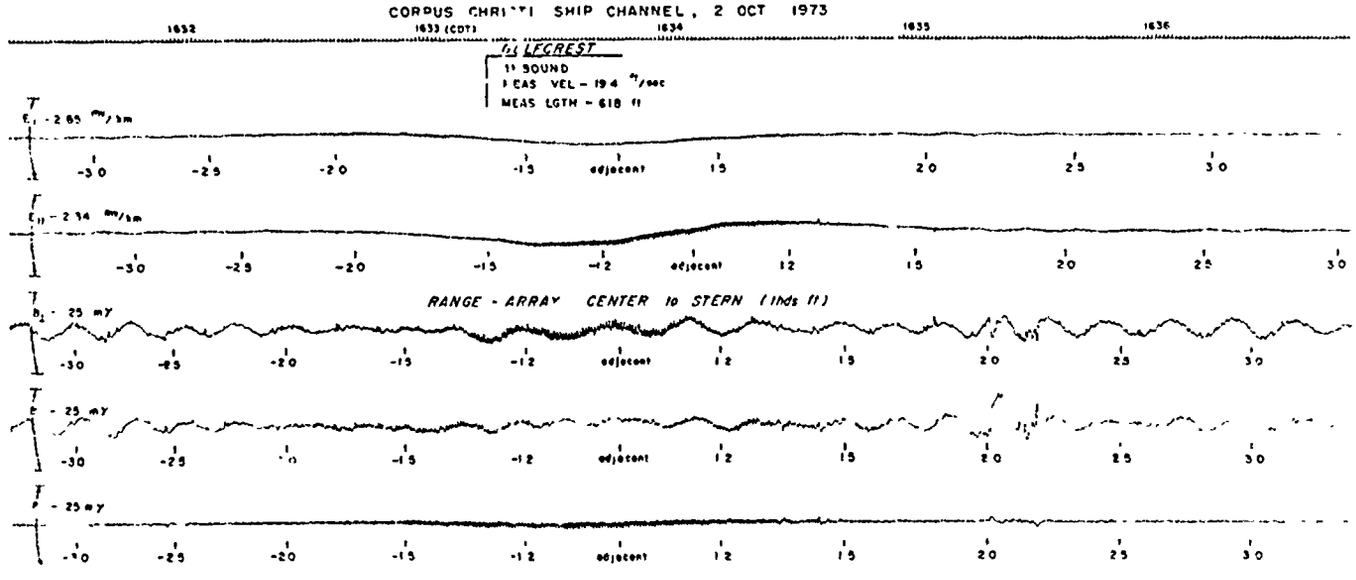

Figure 11. Recorded Time Traces - Gulfcrest

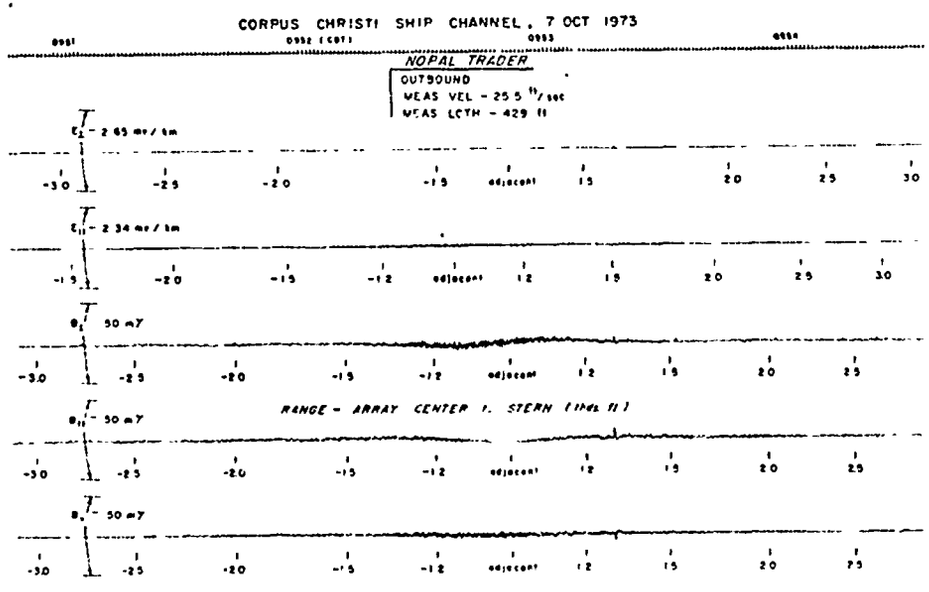

Figure 12. Recorded Time Traces - Nopal Trader

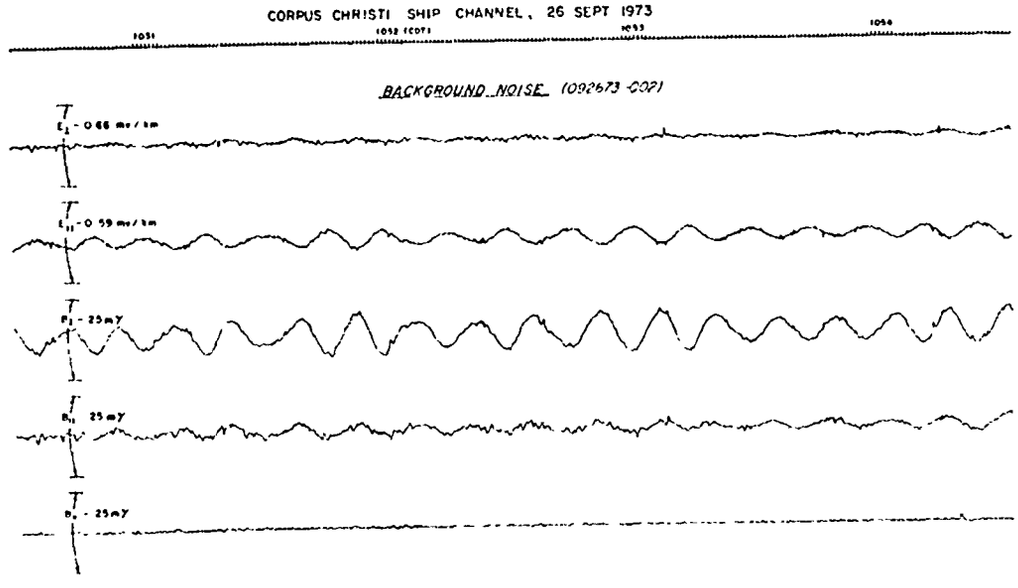

Figure 13. Recorded Time Traces - Background Noise Run 092673-002

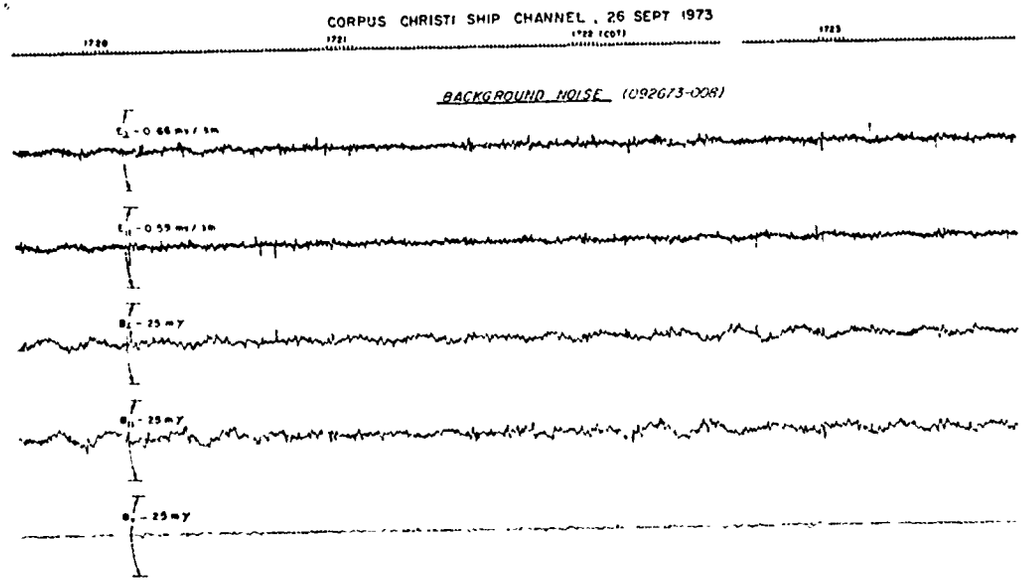

Figure 14. Recorded Time Traces - Background Noise Run 092673-008

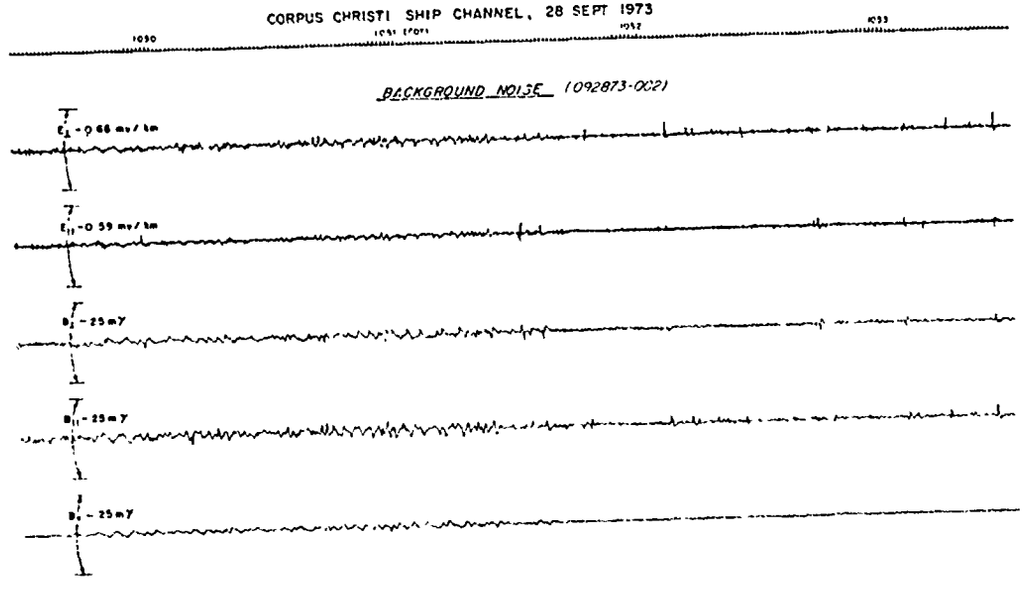

Figure 15. Recorded Time Traces - Background Noise Run 092873-002

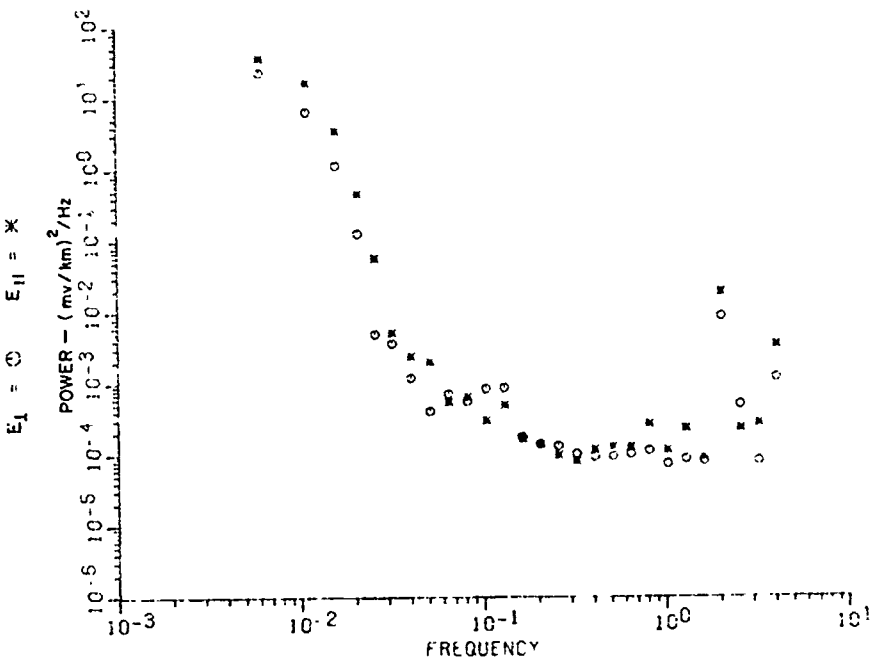

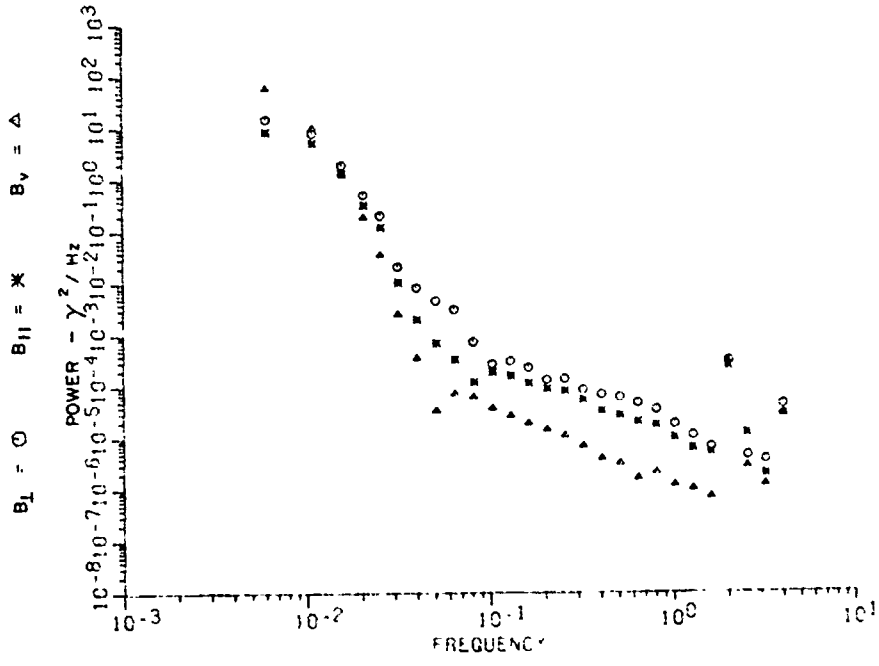

Fig. 16 Stainless Trader (Power Spectra)

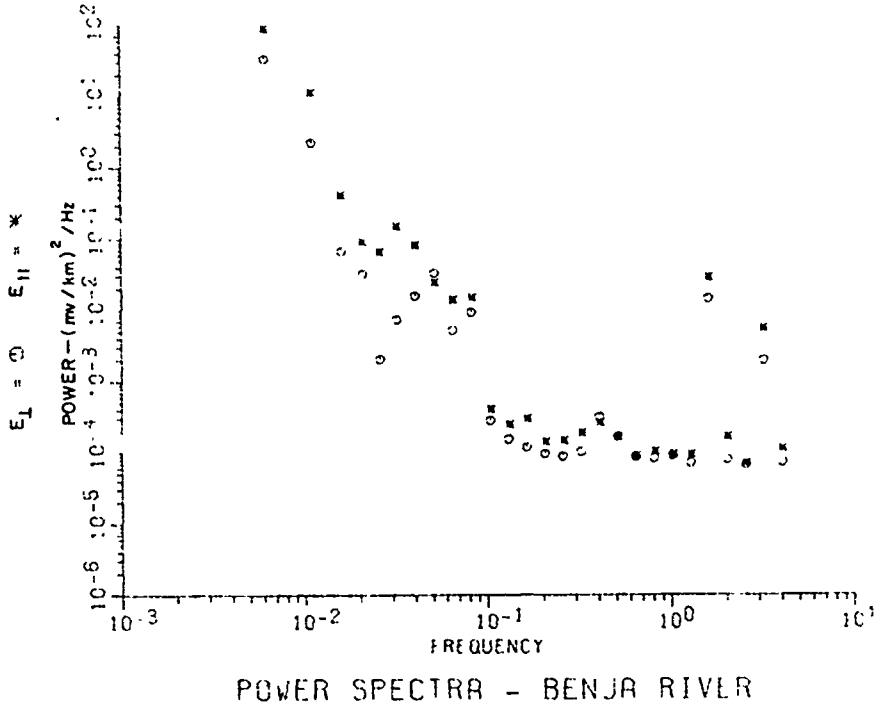

POWER SPECTRA - BENJA RIVER

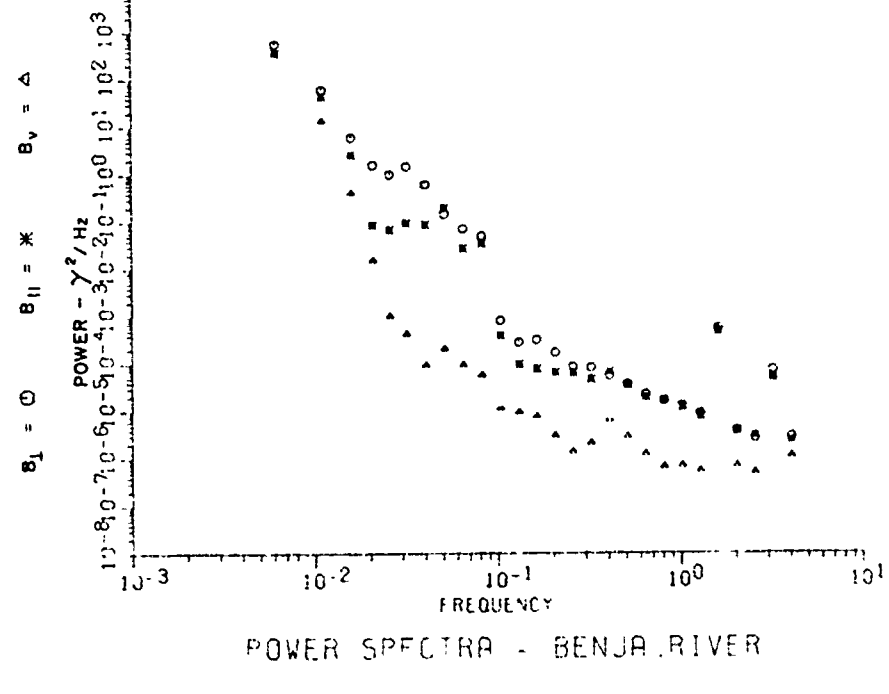

POWER SPECTRA - BENJA RIVER

Fig. 17 Benja River (Power Spectra)

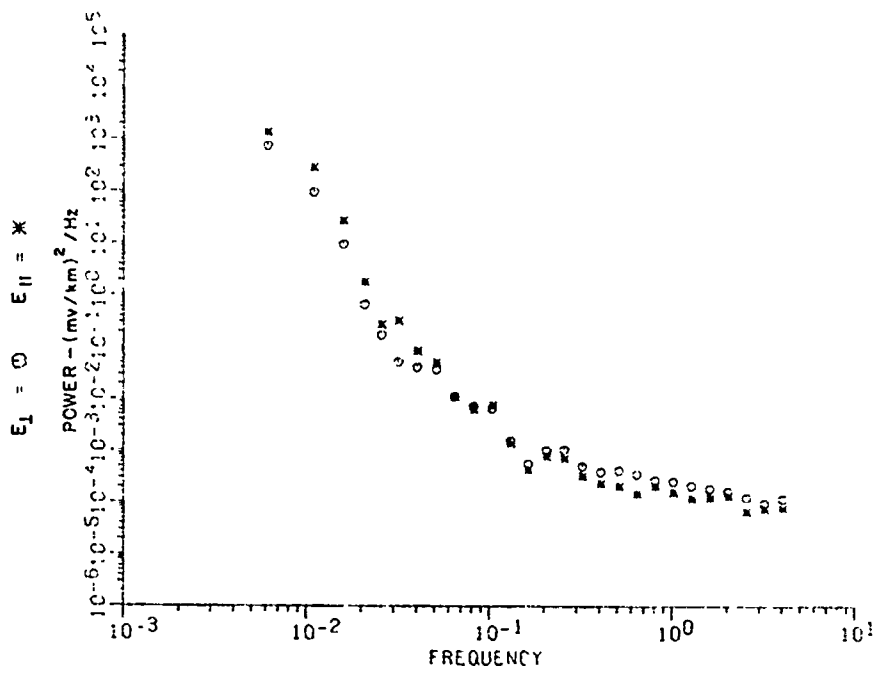

POWER SPECTRA - PITRIA STAR

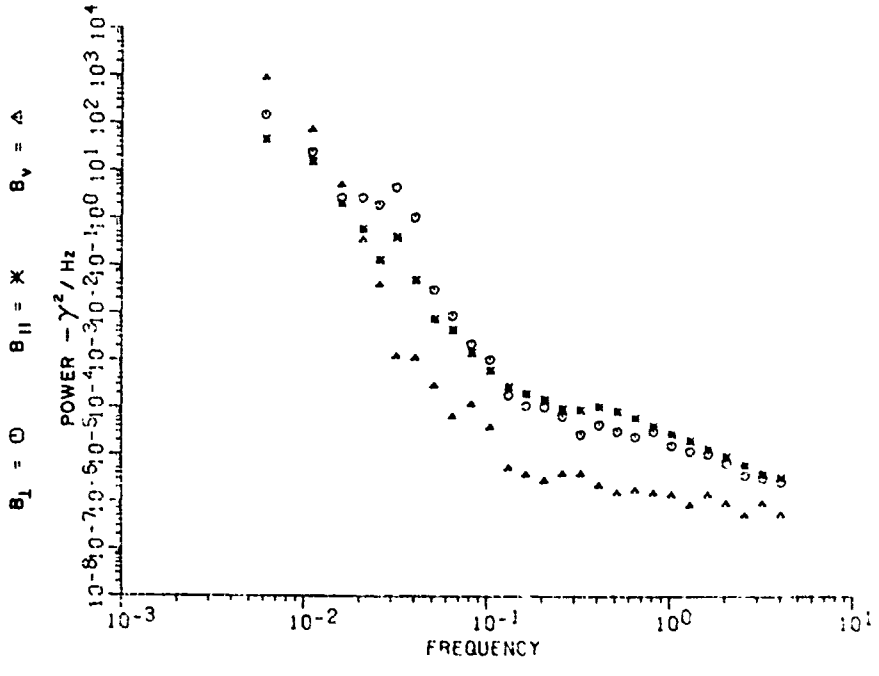

POWER SPECTRA - PITRIA STAR

Fig. 18 Pitra Star (Power Spectra)

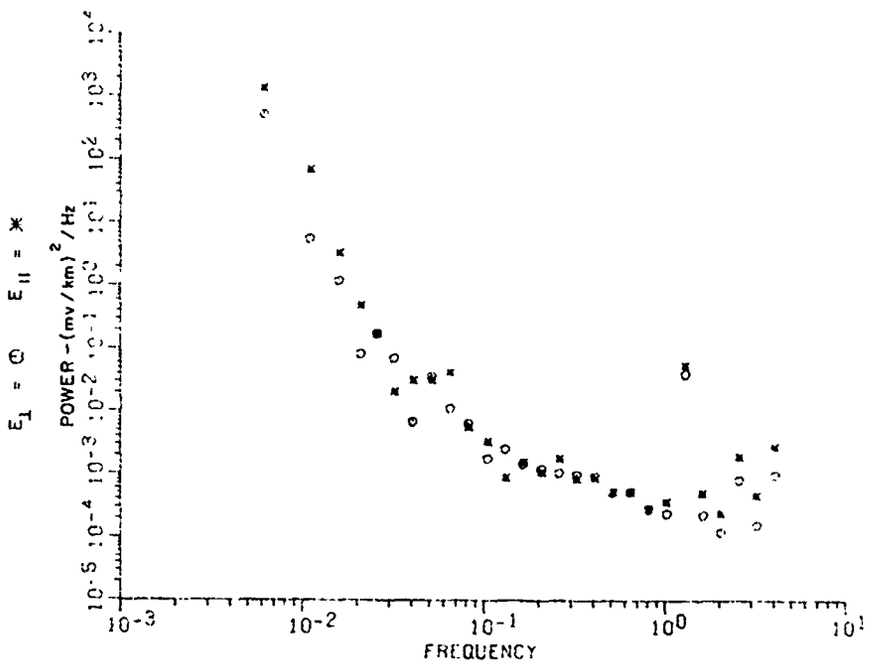

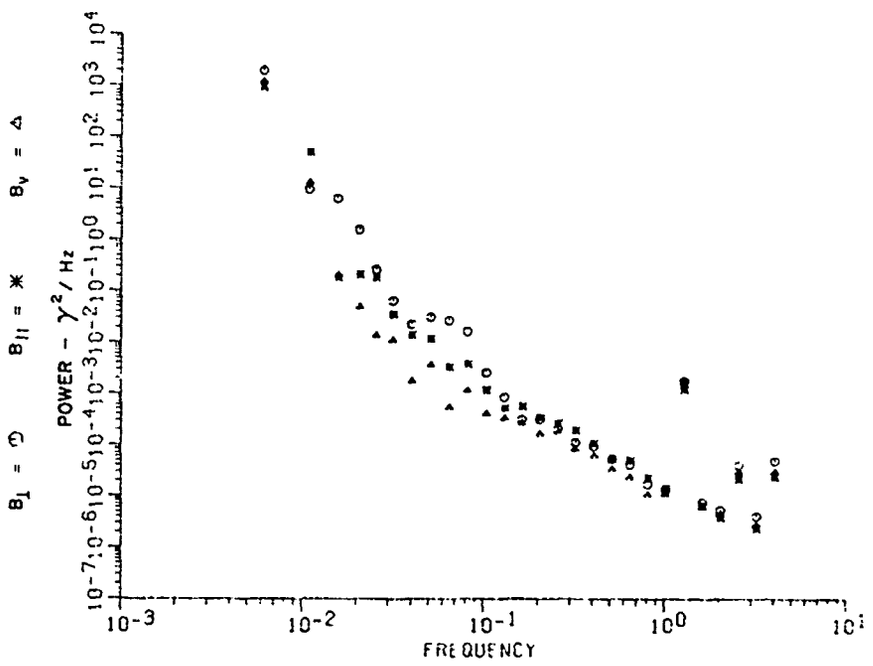

Fig. 19 Inger (Power Spectra)

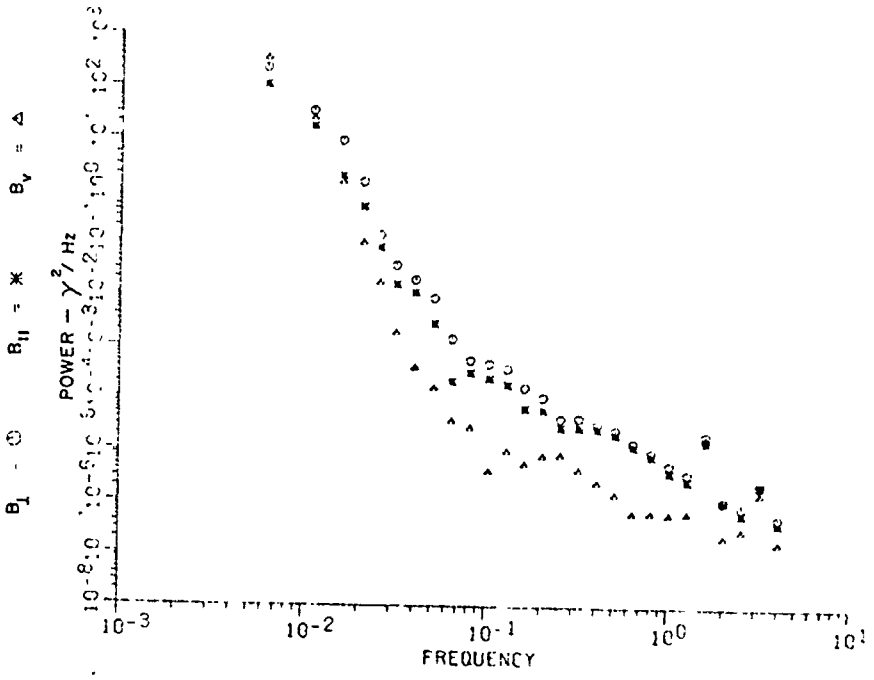

Fig. 20 Tumi (Power Spectra)

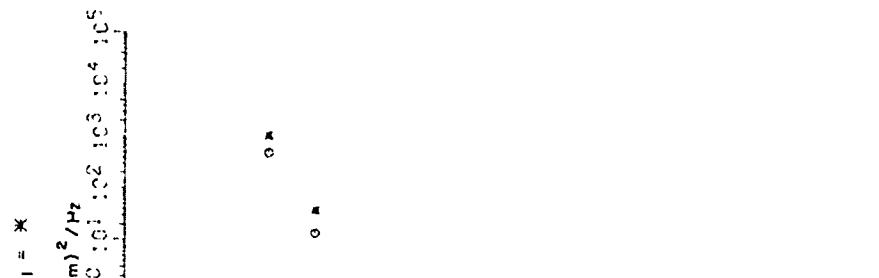

POWER SPECTRA - TEXAS SUN

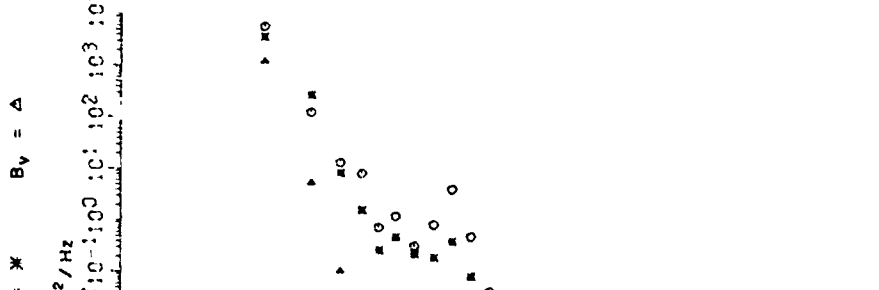

POWER SPECTRA - TEXAS SUN

Fig. 21 Texas Sun (Power Spectra)

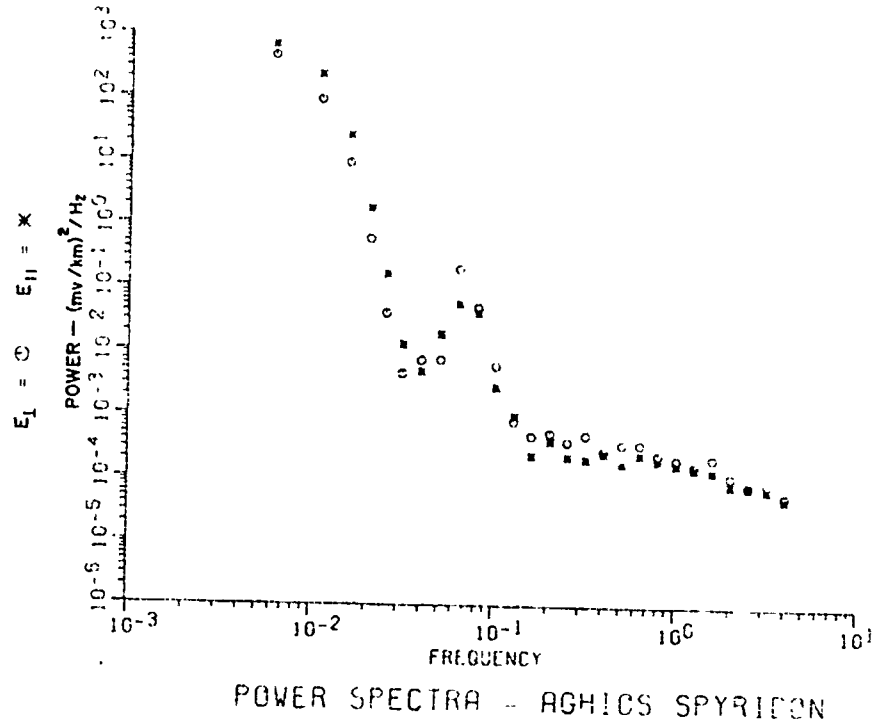

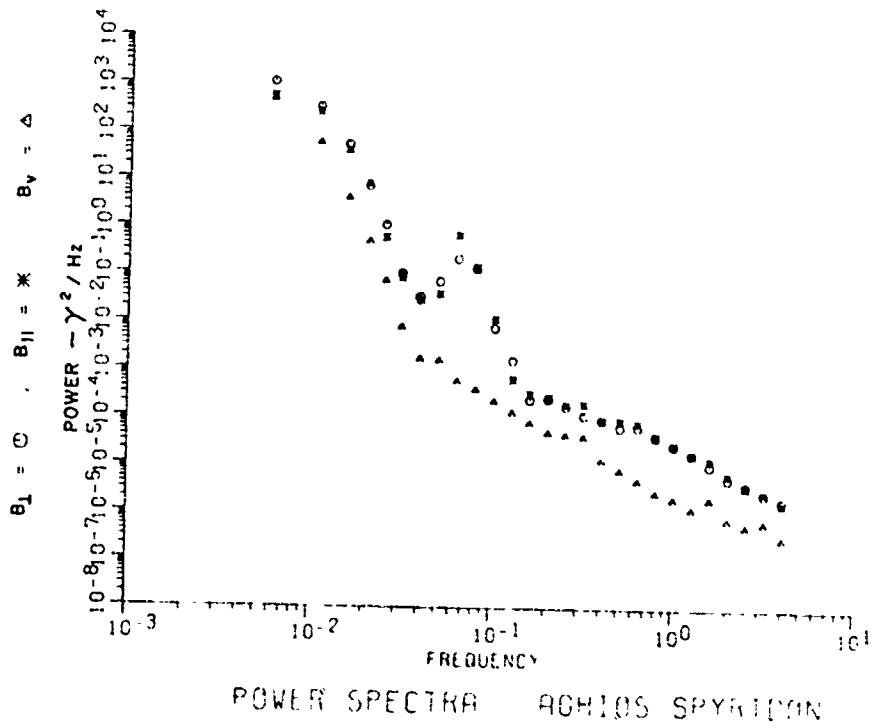

Fig. 22 Aghios Spyridon (Power Spectra)

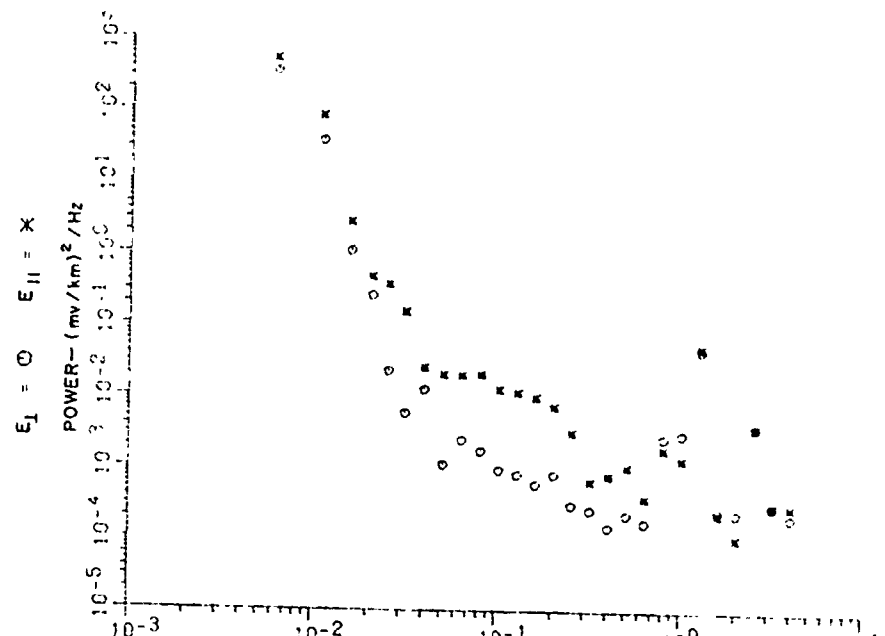

POWER SPECTRA - MARIOTTE

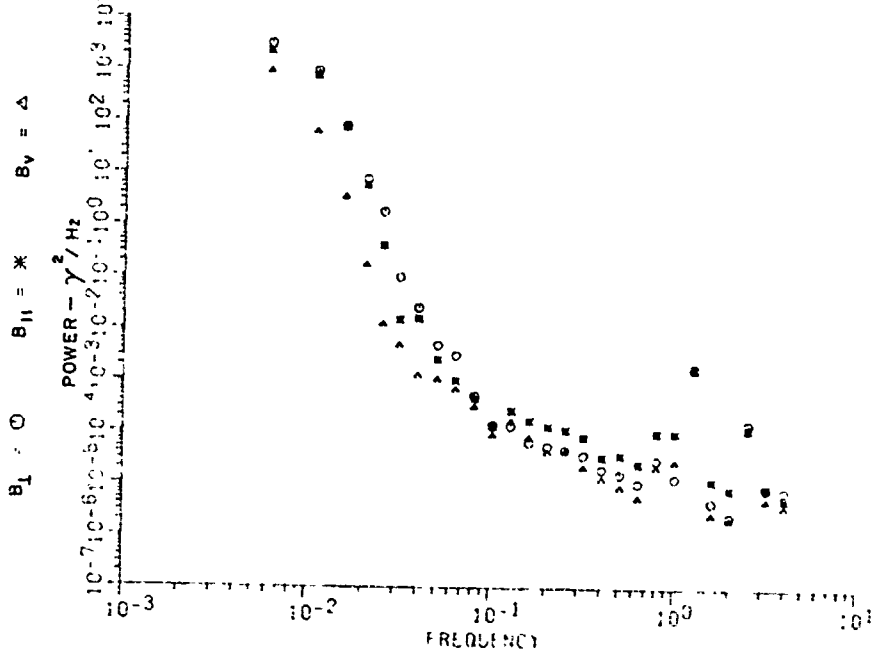

POWER SPECTRA - MARIOTTE

Fig. 23 Mariotte (Power Spectra)

POWER SPECTRA - GULFCREST

POWER SPECTRA - GULFCREST

Fig. 24 Gulfcrest (Power Spectra)

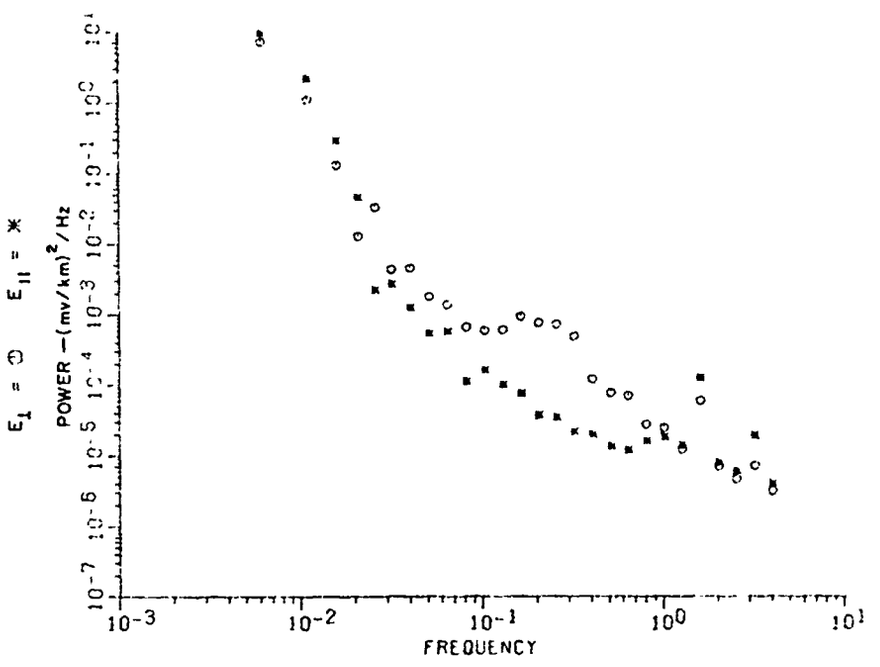

POWER SPECTRA - NOPAL TRADER

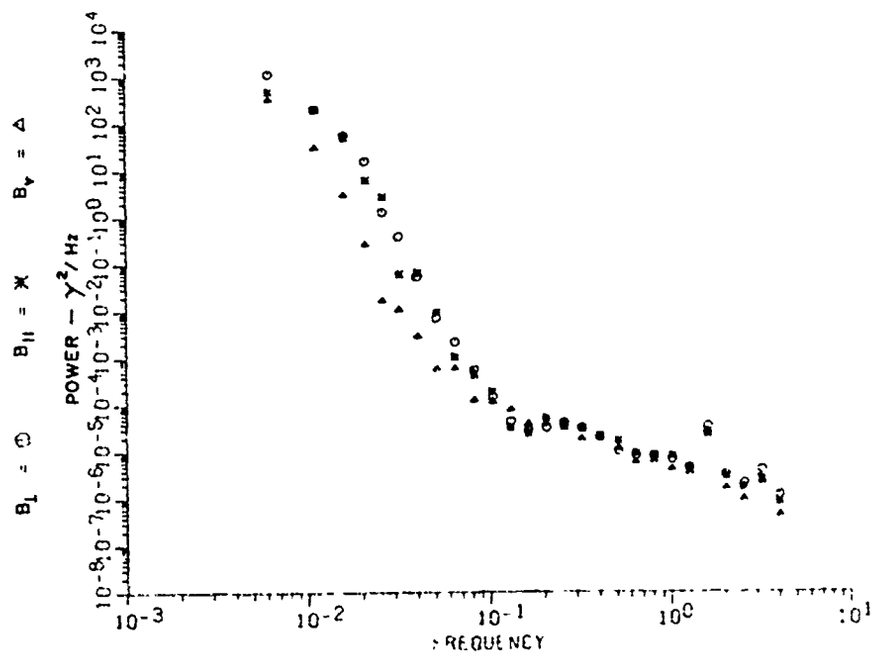

POWER SPECTRA - NOPAL TRADER

Fig. 25 Nopal Trader (Power Spectra)

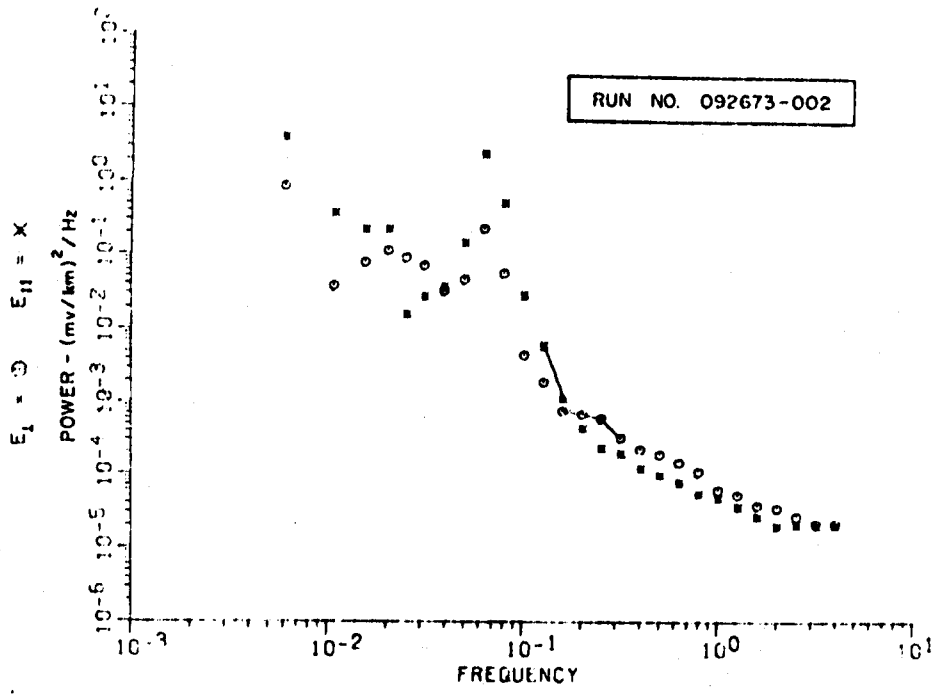

POWER SPECTRA - BACKGROUND RUN

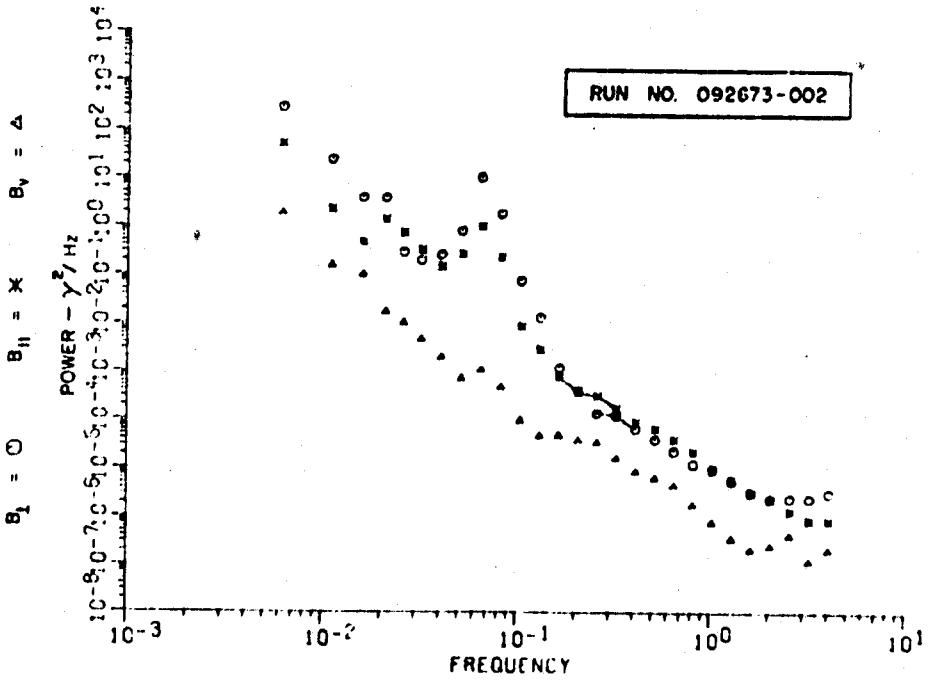

POWER SPECTRA - BACKGROUND RUN

Figure 26. Background Noise 092673-002

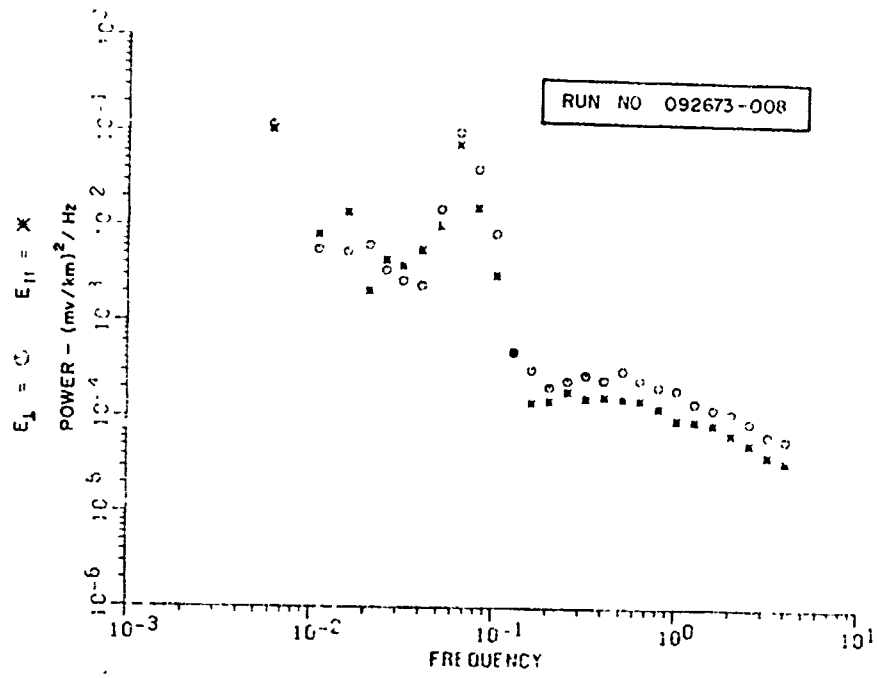

POWER SPECTRA - BACKGROUND RUN

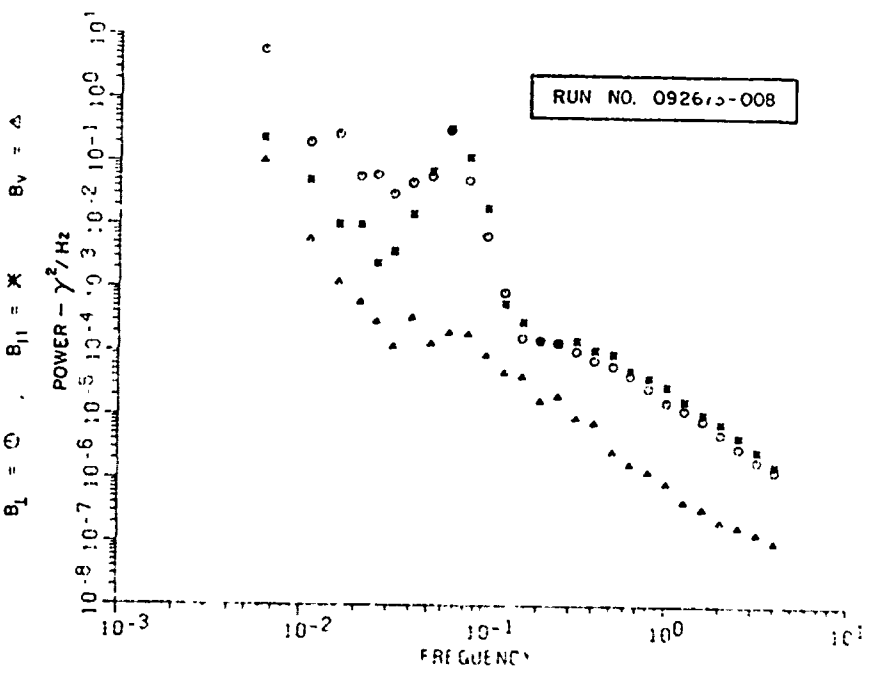

POWER SPECTRA - BACKGROUND RUN

Figure 27. Background Noise 092673-008

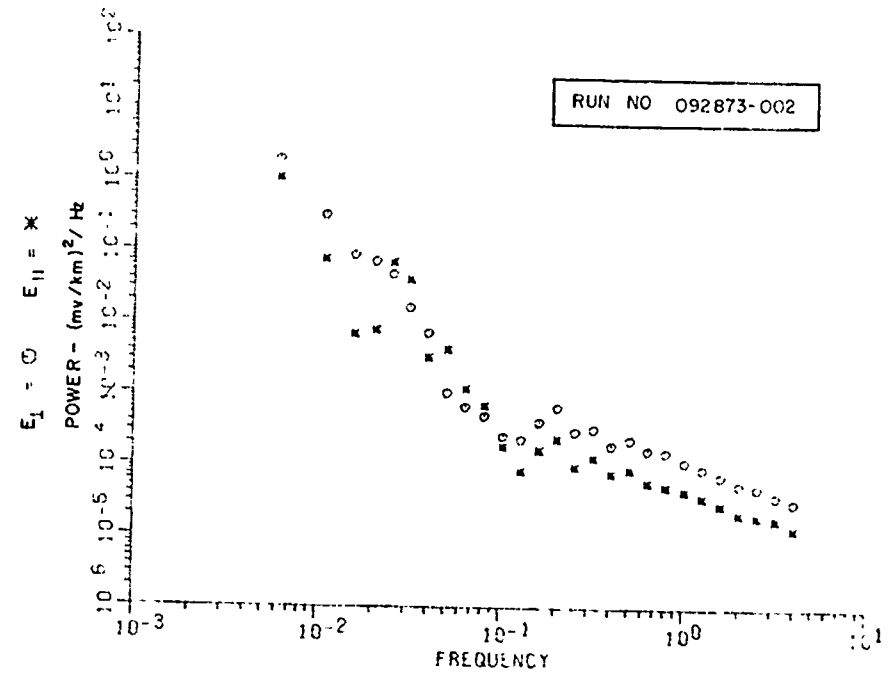

POWER SPECTRA - BACKGROUND RUN

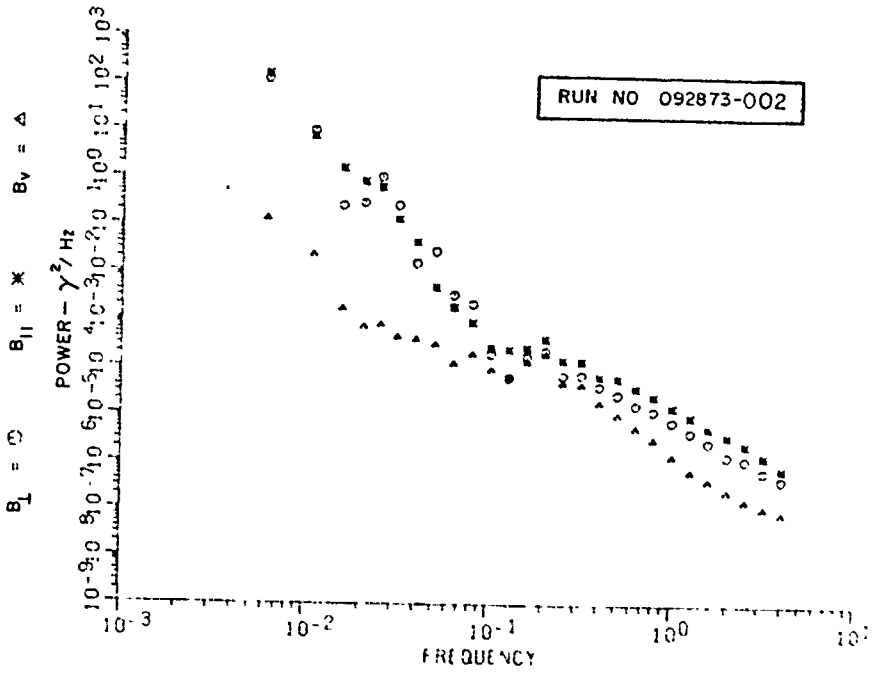

POWER SPECTRA - BACKGROUND RUN

Figure 28. Background Noise 092873-002

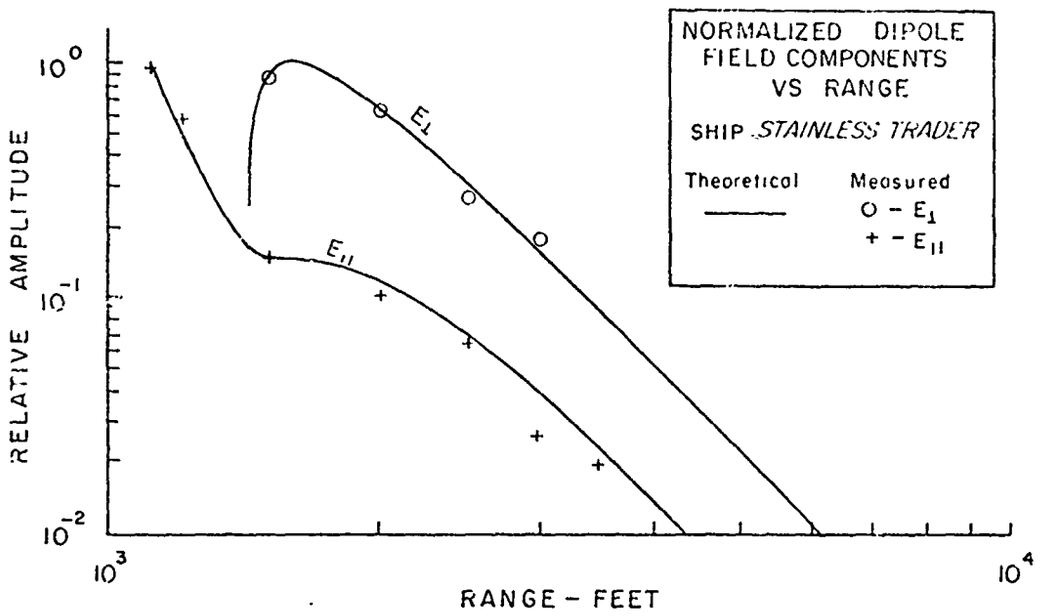

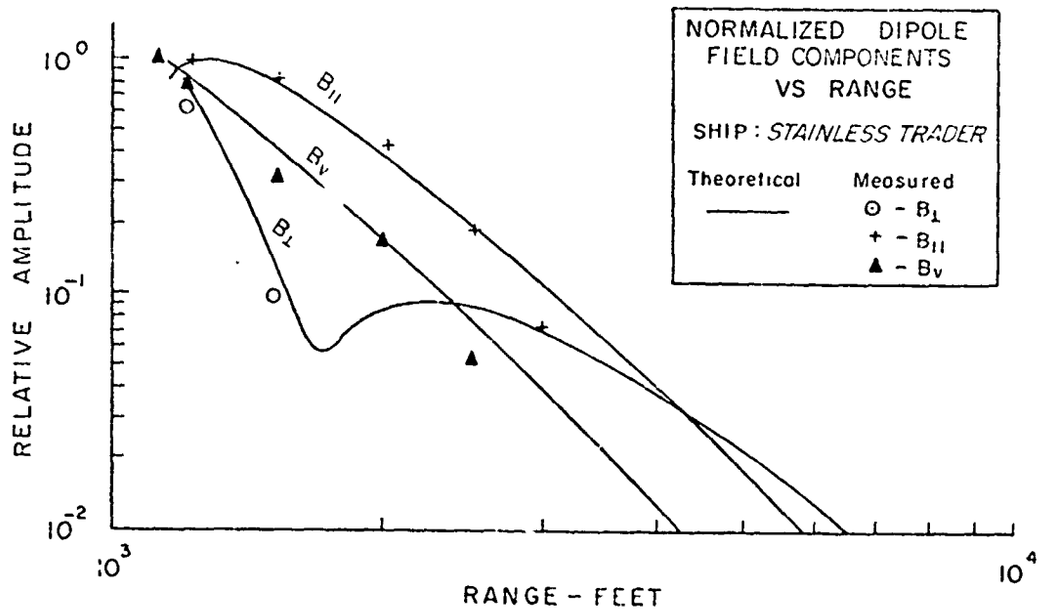

Figure 29. Comparison of Measured and Computed Signals

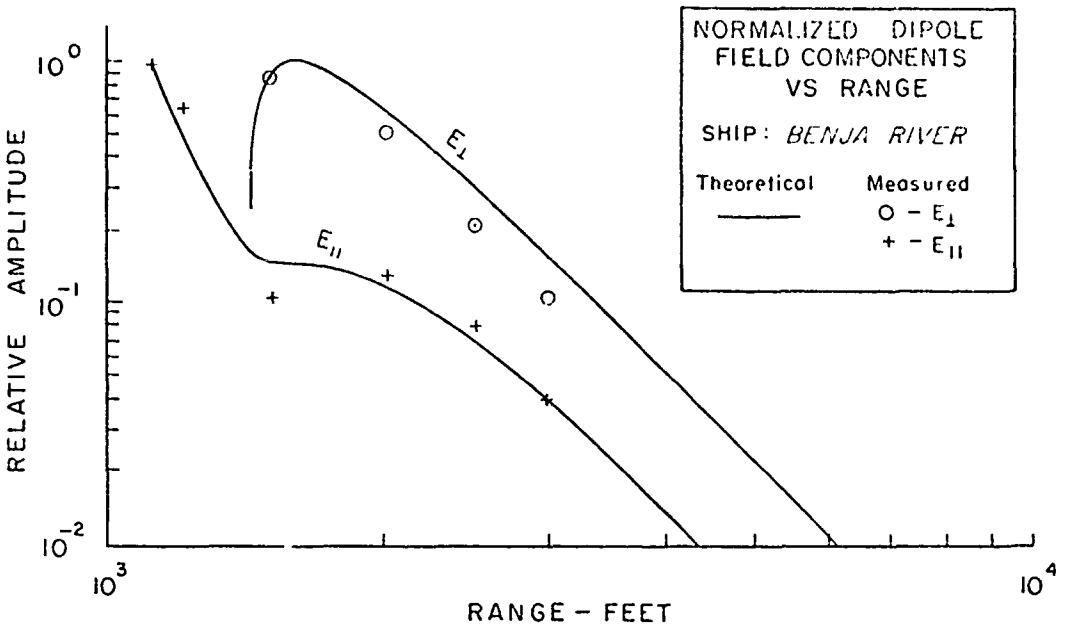

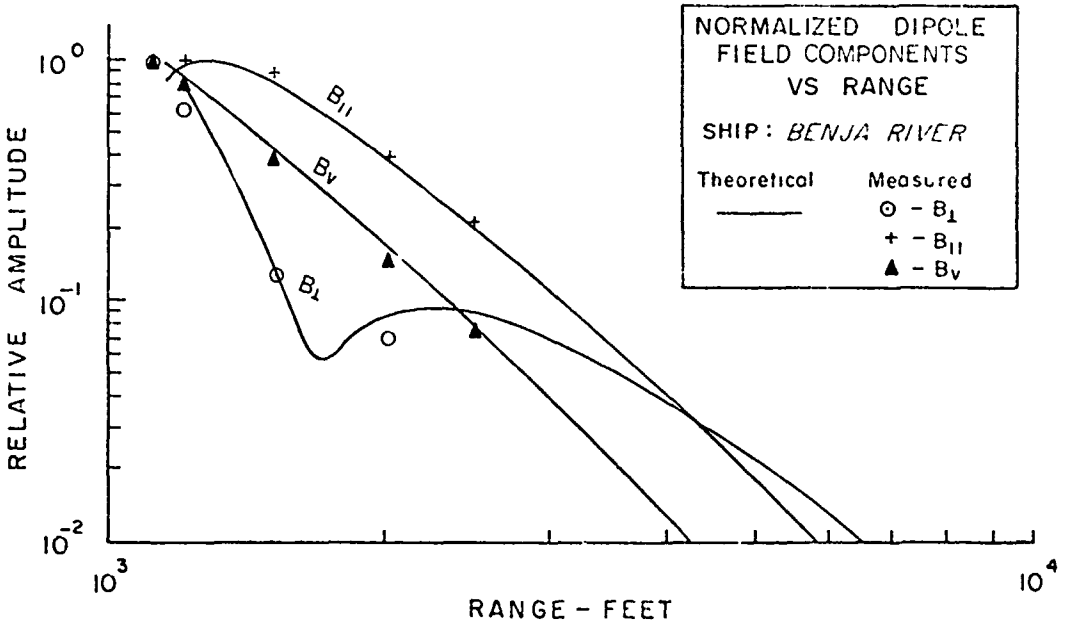

Figure 30. Comparison of Measured and Computed Signals

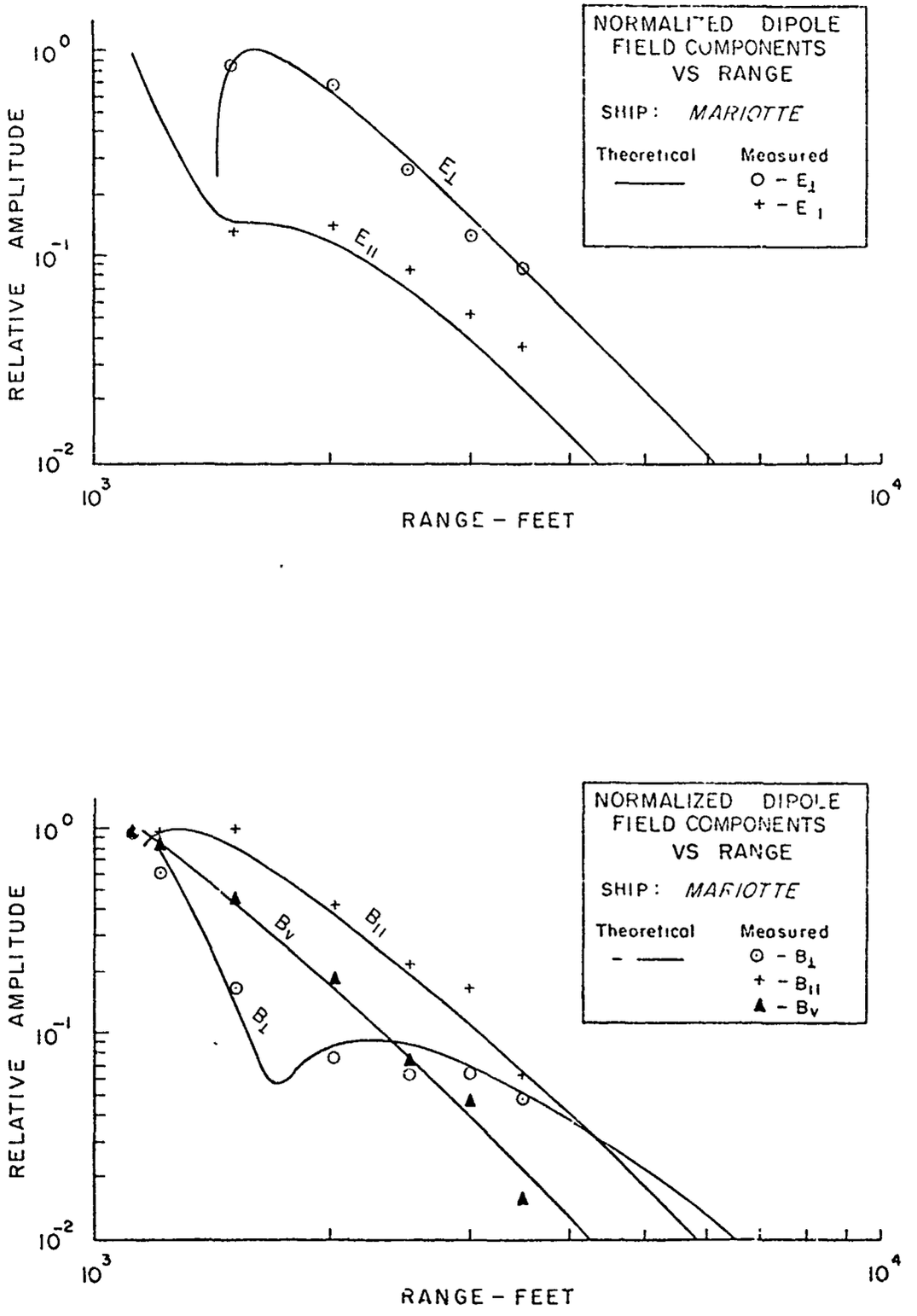

Figure 31. Comparison of Measured and Computed Signals

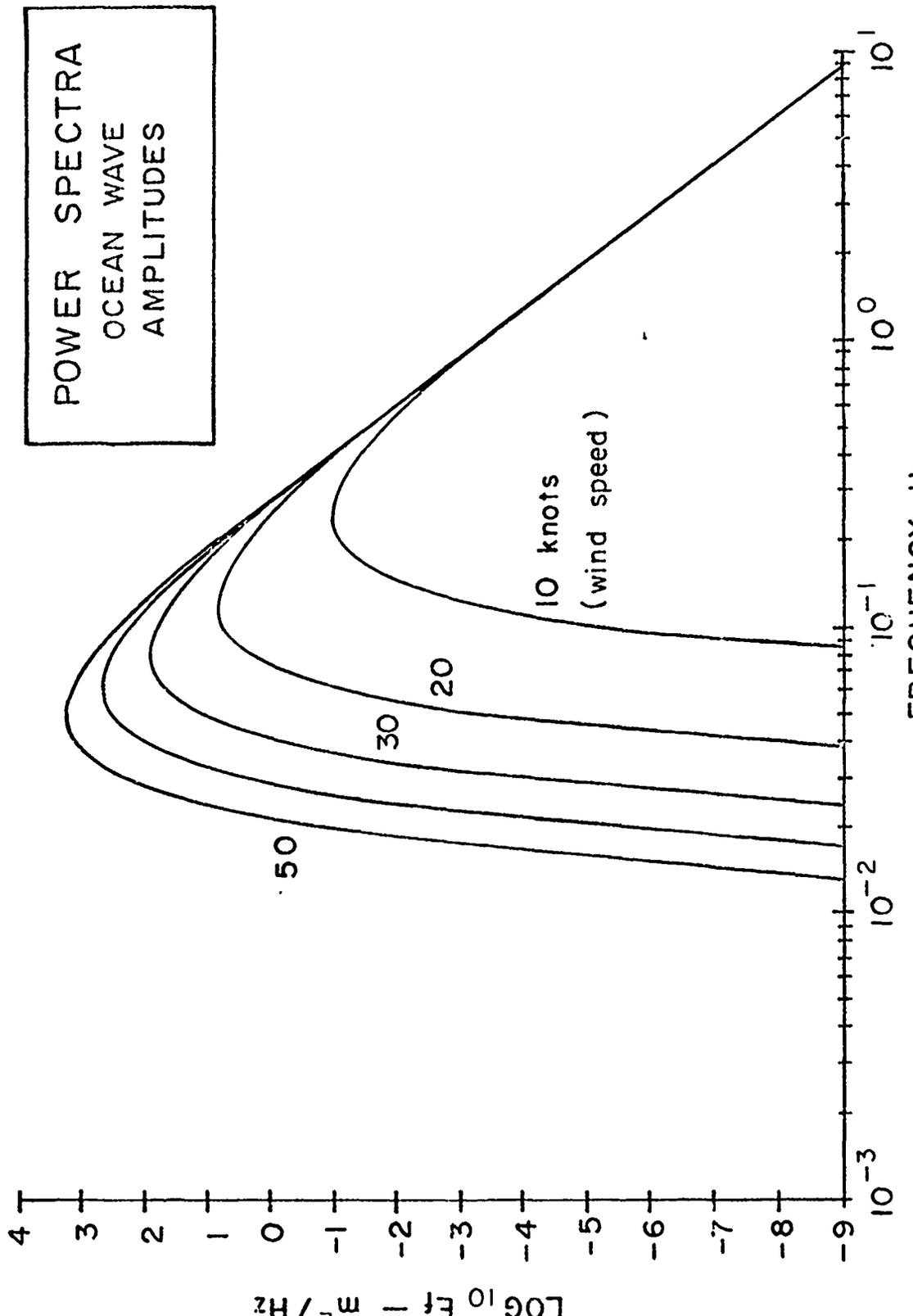

Fig. 32 Wave Noise (E_f)

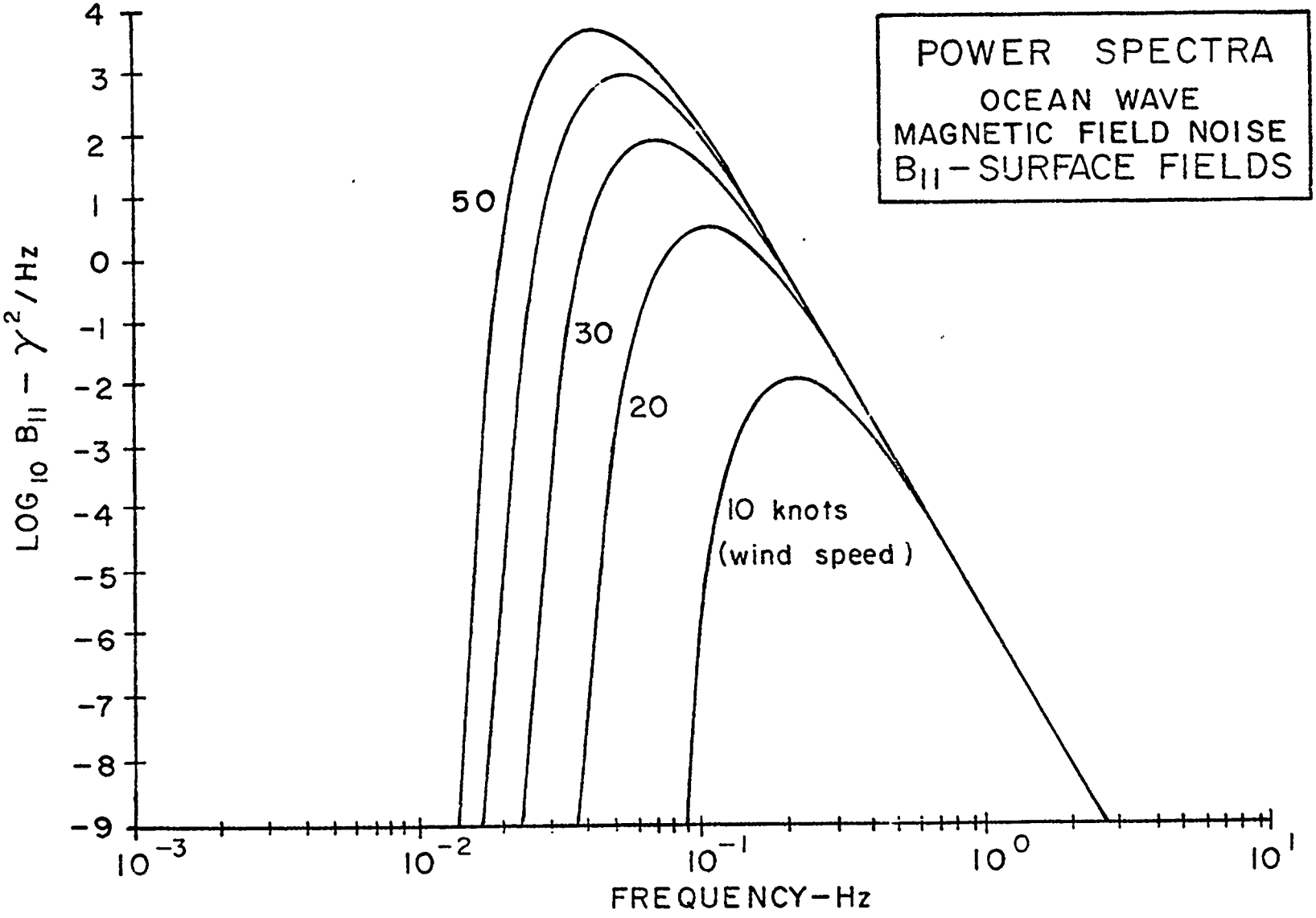

Fig. 33 Wave Noise (B_{11} -Surface)

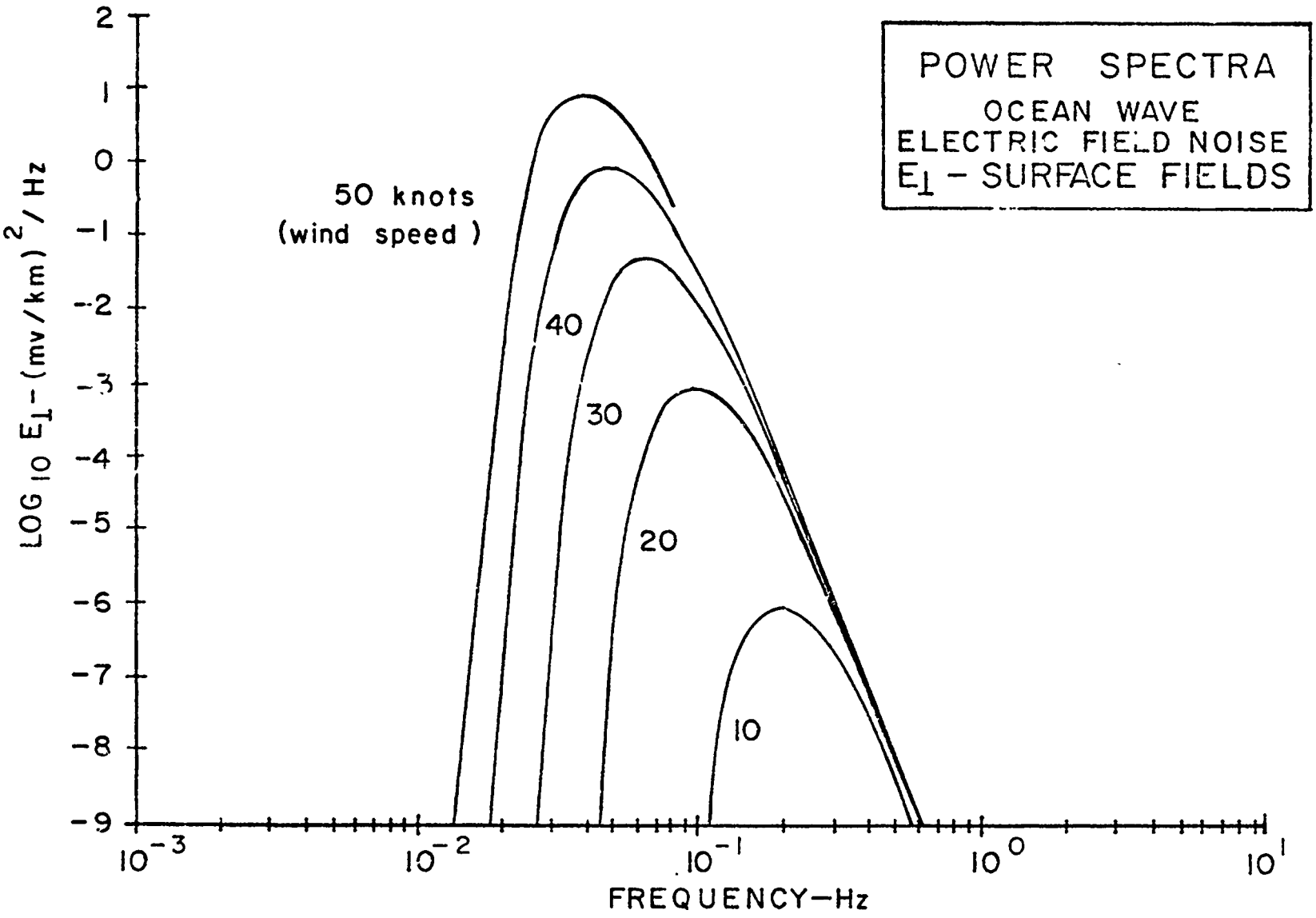

Fig. 34 Wave Noise ($E_\perp$-Surface)

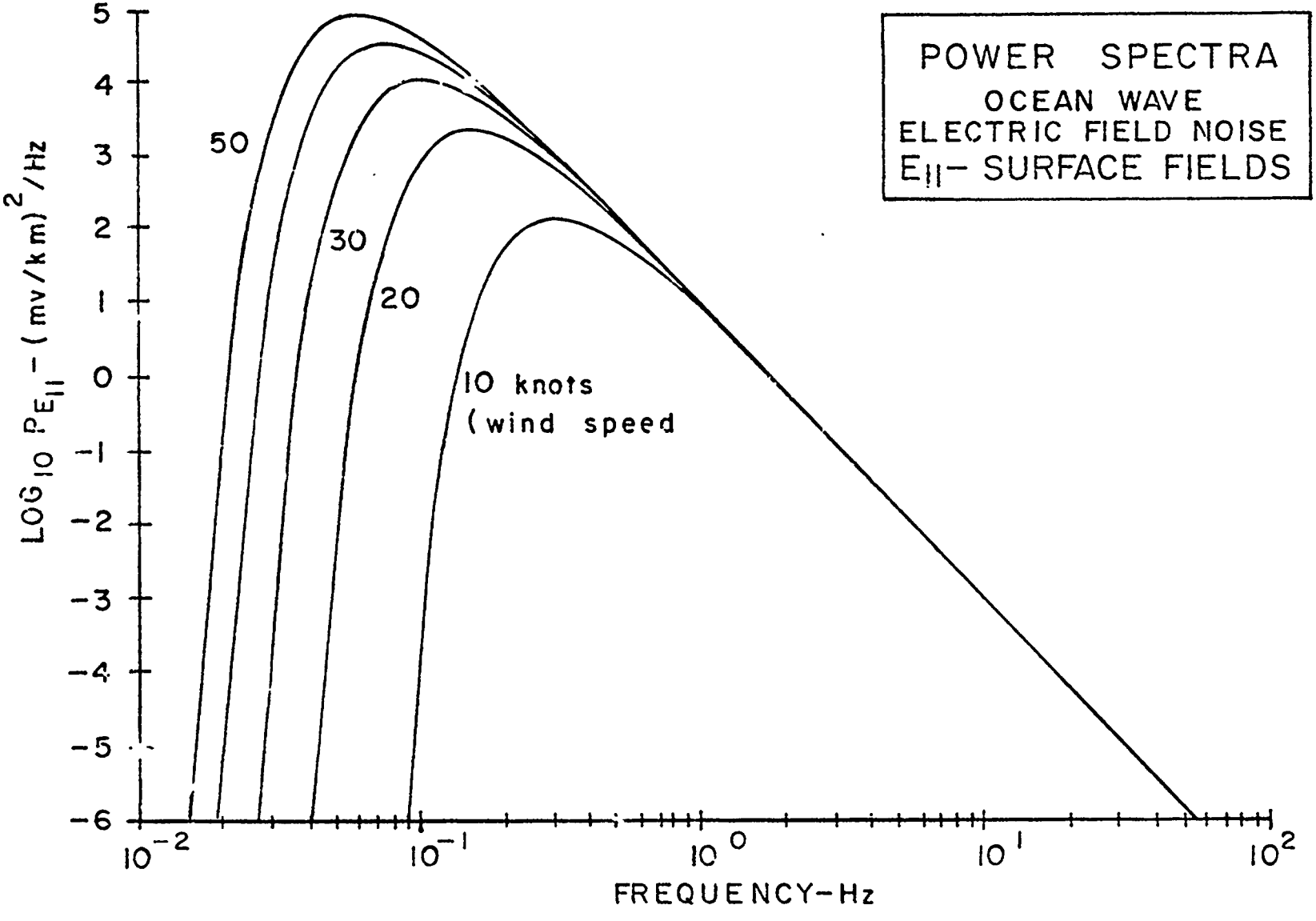

Fig. 35 Wave Noise (E_{11} -Surface)

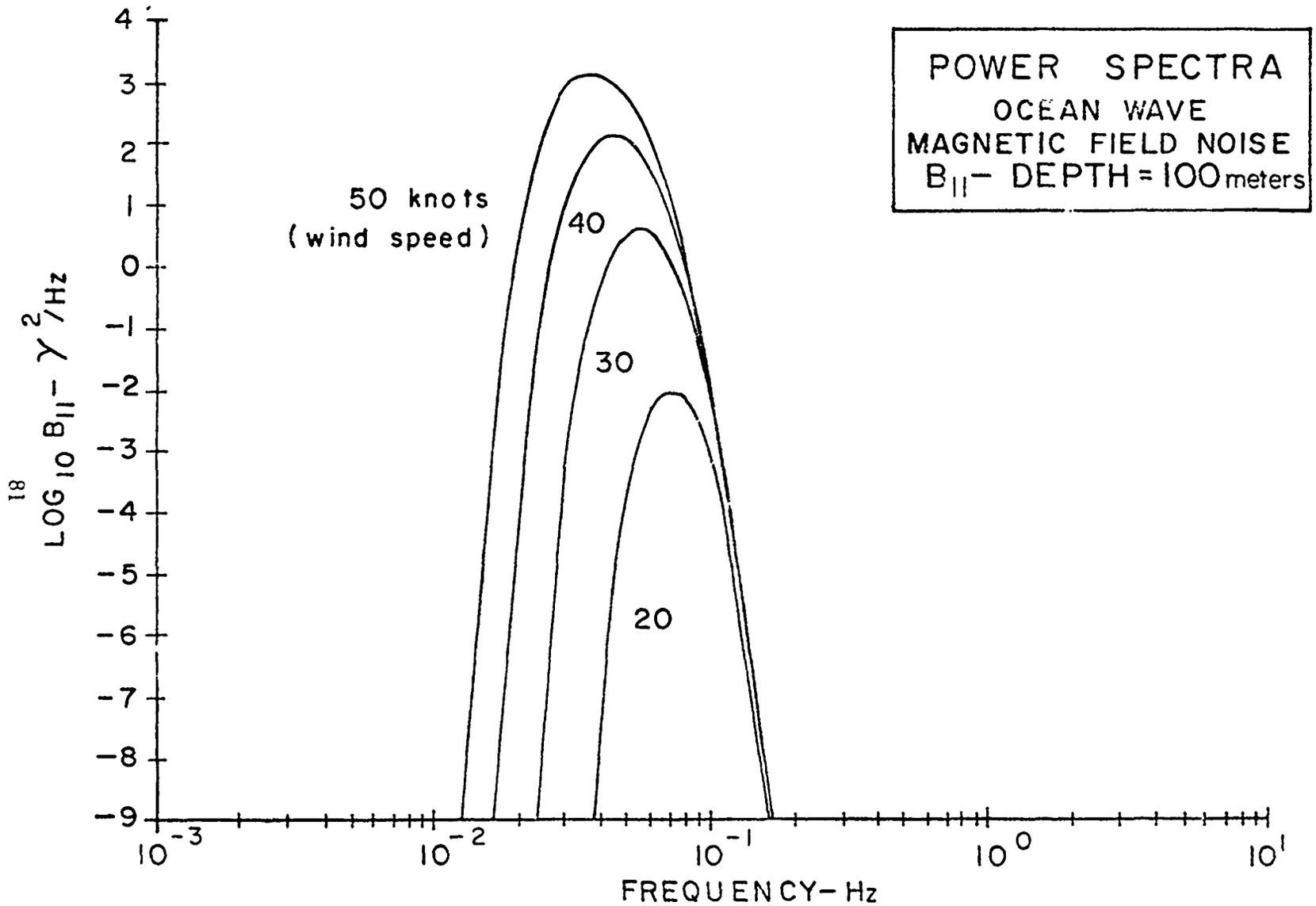

Fig. 36 Wave Noise (B_{11}-Depth=100 M)

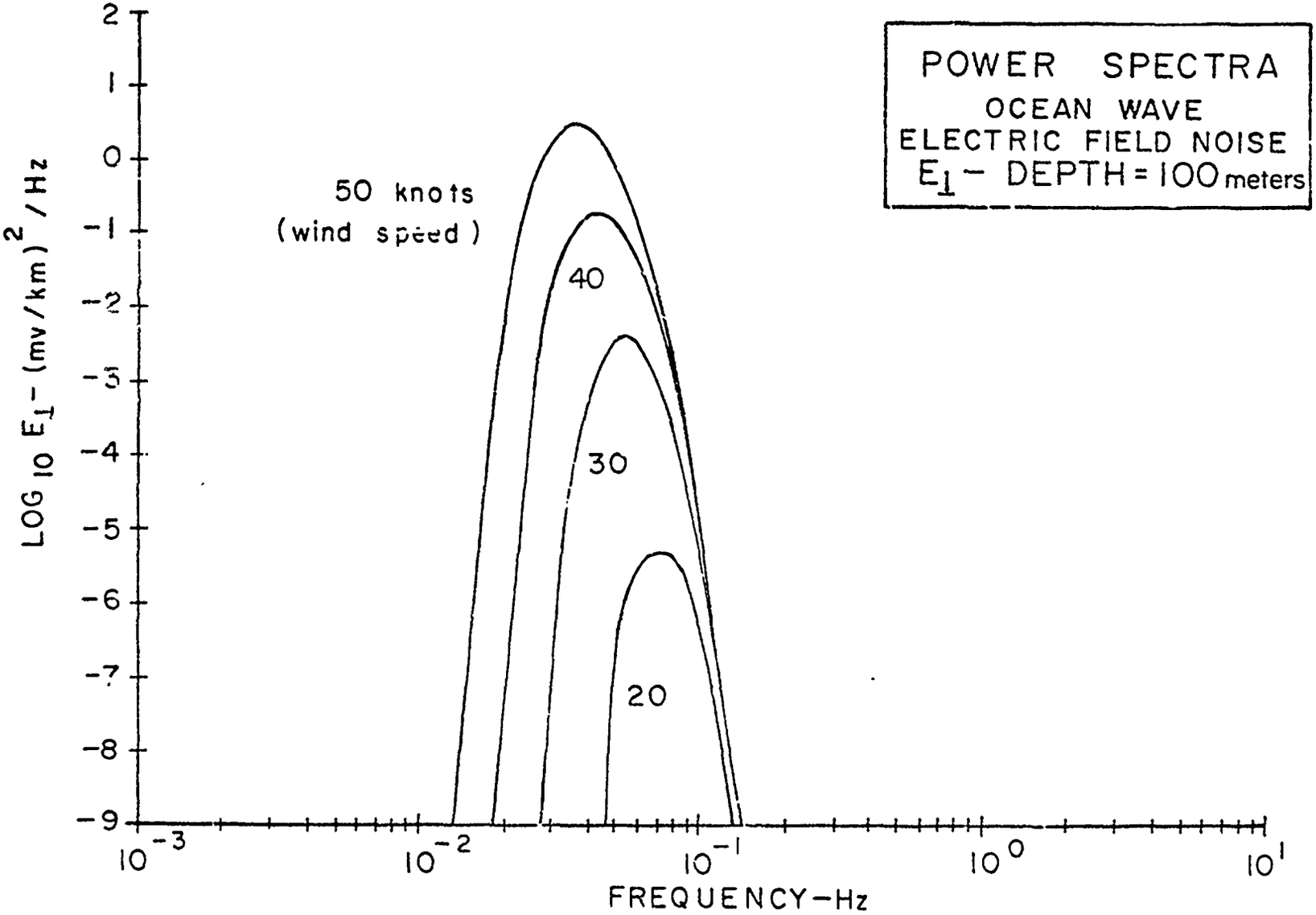

Fig. 37 Wave Noise ($E_\perp$-Depth =100 M)

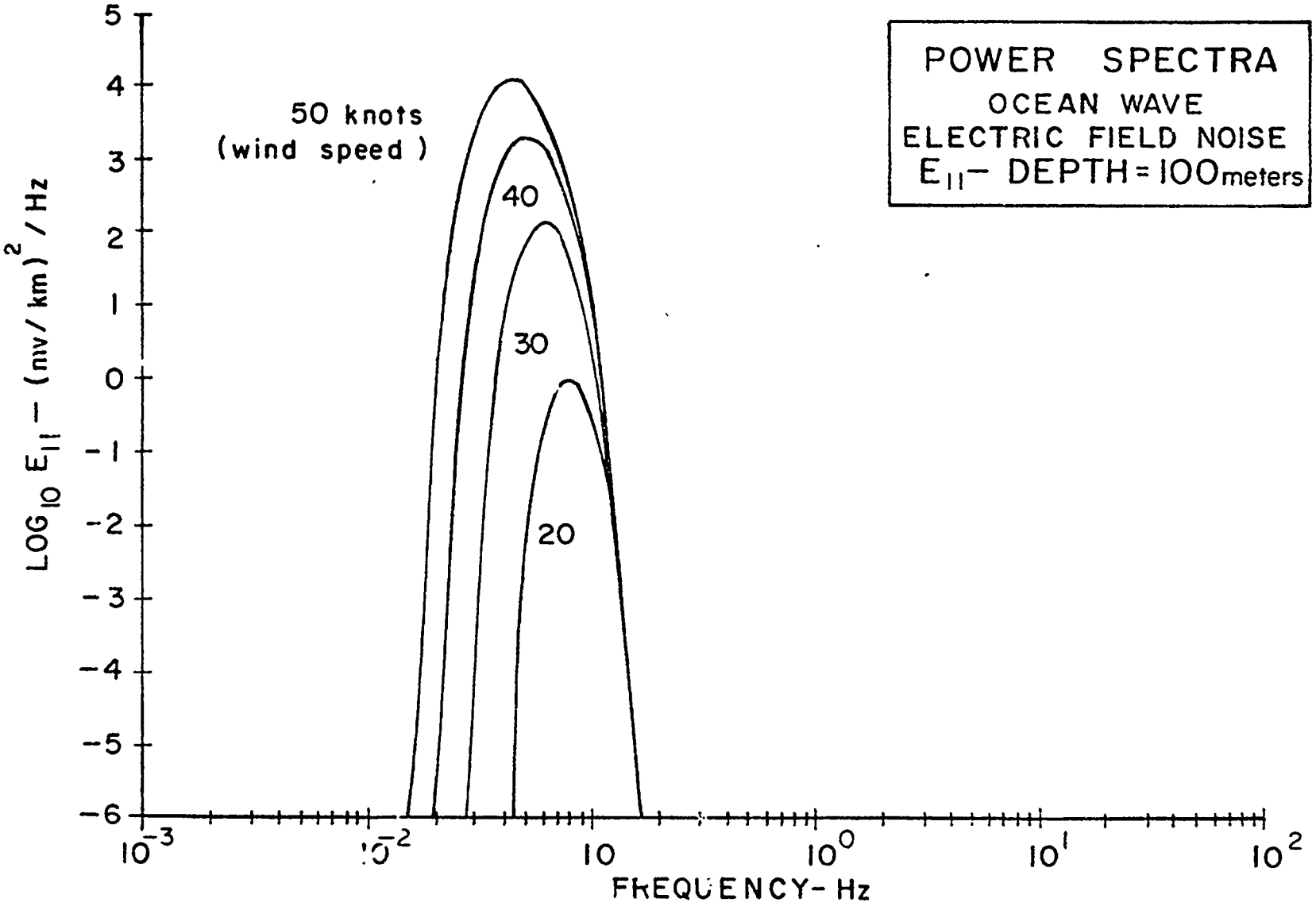

Fig. 38 Wave Noise (E_{11}-Depth =100 M)

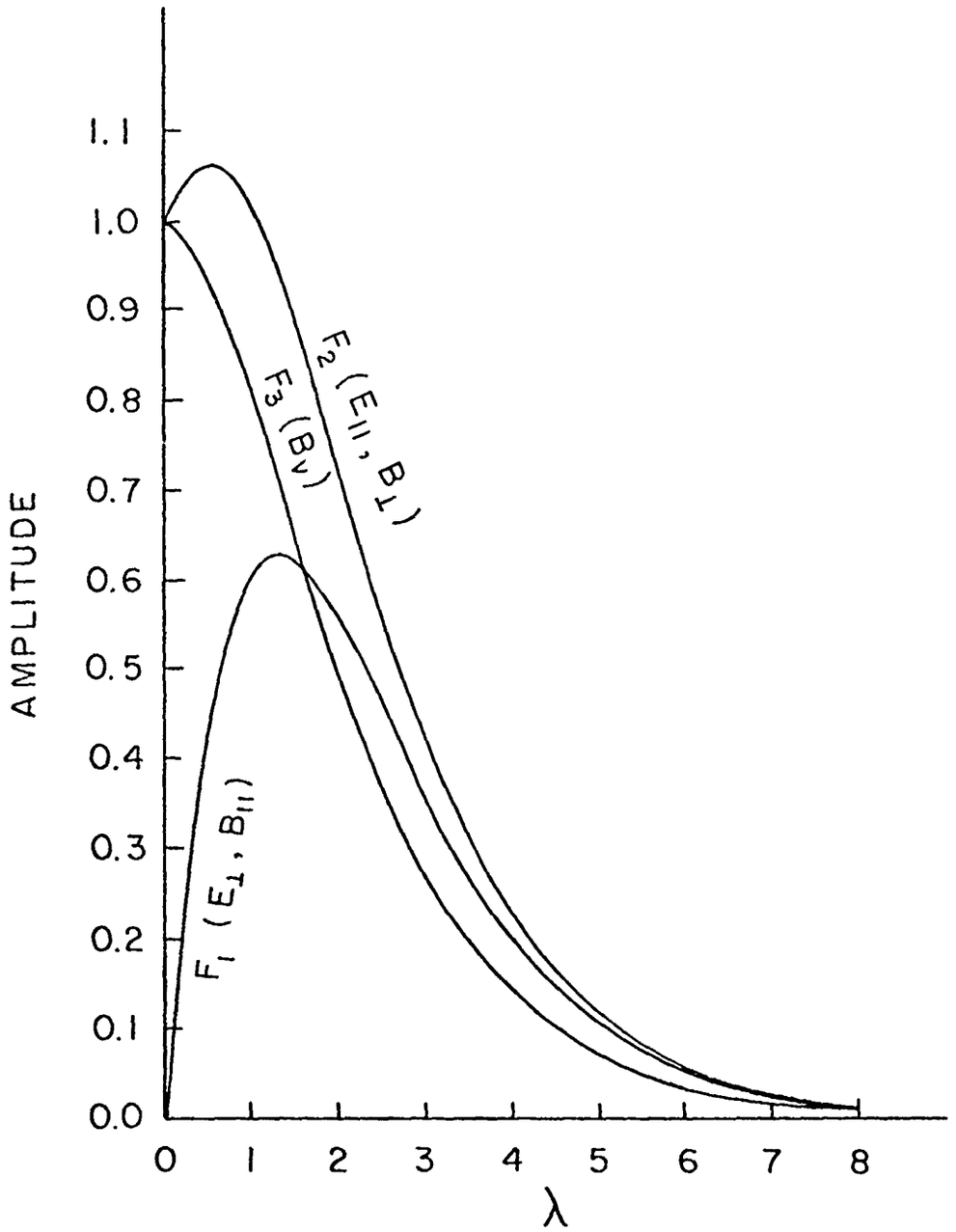

Fig. 39 Matched Filter Shape Functions

REFERENCES

Bannister, P.R., Quasi-Static Fields of Dipole Antennas at the Earth's Surface, Radio Science, Vol. 1 (New Series), No. 11, 1321-1330, November 1966.

Bateman, H., Tables of Integral Transforms, Vol. I, McGraw Hill, 1954.

Brunk, Mathematical Statistics, Blaisdell Publishing Co., 1965.

Defant, A., Physical Oceanography, Volume II, Permagon Press, 1961.

Dwight, H.D., Tables of Integral and Other Mathematical Data, Third Edition, McGraw Hill, 1961.

Fowler, B.C. et al, Magnetic Anomaly Detection Utilizing Component Differencing Techniques, Technical Report No. 154, Electronics Research Center, U.T. Austin, August 1973.

Kraichman, M. B., Handbook of Electromagnetic Propagation in Conducting Media, NAVMAT P-2302, U.S. Government Printing Office, 1970.

Podney, W., Electromagnetic Noise Induced by Ocean Waves: I. Electromagnetic Field Induced by Progressive Ocean Waves, RADC-TR-74-131, Technical Report, March 1974.

Podney. W., Electromagnetic Fields Generated by Ocean Waves, RADC-TR-74-285, Final Technical Report, August 1974.

Weaver, J. T., Magnetic Variations Associated With Ocean Waves and Swell, J. Geophysics Res., 70, 1921-1929, 1965.

CONFERENCE PROCEEDINGS

Ocean Wave Spectra, Proceedings of a Conference, sponsored by the U.S. Naval Oceanographic Office and Division of Earth Sciences, National Academy of Sciences, National Research Council, Easton, Md., May 1-4, 1961, Prentice-Hall, 1963.

Appendix
Wave Noise Derivation

Expressions for the electric and magnetic fields generated by ocean wave motions of the conductive sea water perpendicular to the geomagnetic field are derived in this appendix. The derivation assumes that the ocean wave motions are described by the simple Airy theory of surface waves. No attempt has been made to include the effects of internal waves. For other treatments of the electromagnetic fields generated by ocean waves, the reader is referred to references [Weaver, 1965], [Beal and Weaver, 1970], [Podney, 1974A], [Podney, 1974B].

Simple Airy wave theory assumes that the air sea interface varies sinusoidally about mean sea level with respect to both time and horizontal distance. If the position of the surface with respect to mean sea level is designated by η, then

$$\eta(x,t) = ae^{j(\omega t - kx)}$$

This represents a wave propagating in the +x direction whose motions are independent of y as illustrated in Figure 1A. If v represents the velocity of the water at any point below the surface, we may write

$$\bar{v} = \bar{a}_x u + \bar{a}_z w$$

The Airy wave theory assumes that the flow of water associated with the wave is irrotational expressed by

$$\nabla \times \bar{v} = 0$$

and that the water is incompressible, expressed by

$$\nabla \cdot \bar{v} = 0 \qquad \text{A-1}$$

The assumption of irrotational flow suggests the use of a scalar velocity potential, ψ, given by

$$v = -\nabla \psi \qquad \text{A-2}$$

Substituting A-2 into A-1 gives La Place's equation,

$$\nabla^2 \psi = 0 \qquad \text{A-3}$$

for the velocity potential.

Solutions of A-3 may be written as

$$\psi = (Ae^{kz} + Be^{-kz})\, e^{j(\omega t - kx)}. \qquad \text{A-4}$$

In order to evaluate A and B we use the known values of the vertical components of the water velocity, w, at $z = 0$ and at $z = -h$. In terms of ψ, w may be expressed as

$$w = -\frac{\partial \psi}{\partial z} = -k(Ae^{kz} - Be^{-kz})e^{j(\omega t - kx)}$$

At $z = 0$,

$$w = \frac{\partial \eta}{\partial t} = j\omega a\, e^{j(\omega t - kx)}$$

so that

$$(A - B) = \frac{-j\omega a}{k} \qquad \text{A-5}$$

At $z = -h$, $\omega = 0$ giving

$$Ae^{-kh} - Be^{kh} = 0 \qquad \text{A-6}$$

Solving A-5 and A-6 for A and B gives

$$A = -\frac{j\omega a e^{kh}}{2k \sinh kh} \qquad \text{A-7}$$

and

$$B = \frac{j\omega a e^{-kh}}{2k \sinh kh} \qquad \text{A-8}$$

Using A-7 and A-8 in A-4 we obtain

$$\Psi = -\frac{j\omega a}{k} \frac{\cosh(z+h)}{\sinh kh} e^{j(\omega t - kx)} \qquad \text{A-9}$$

Substituting this expression for Ψ in A-2 yields for the component velocities

$$u = \omega a \frac{\cosh k(z+h)}{\sinh kh} e^{j(\omega t - kx)}$$

and

$$v = j\omega a \frac{\sinh k(z+h)}{\sinh kh} e^{j(\omega t - kx)}$$

In order to obtain an expression for k in terms of ω (the dispersion relation) we make use of Euler's equation (equation of motion). Thus

$$\rho \frac{d\bar{v}}{dt} = -\rho \nabla u - \nabla p$$

where ρ is the mass density of the water,

$$u = gz + C_1$$

is the gravitational potential with $g \approx 9.81$ m/sec^2 and C_1 a constant; and p is the scalar water pressure. Expanding the total derivative gives

$$\rho\left(\frac{\partial \bar{v}}{\partial t} + \bar{v} \cdot \nabla \bar{v}\right) = -\rho \nabla u - \nabla p$$

We linearize this equation by assuming that the waves have a reasonably small amplitude so that the factor $\bar{v} \cdot \nabla\bar{v}$ is negligible. There remains the equation

$$- \rho \nabla \frac{\partial \Psi}{\partial t} = - \rho \nabla u - \nabla p$$

that may be integrated to obtain

$$- \rho \frac{\partial \Psi}{\partial t} = - \rho g z + C_1 - p + C_2 \qquad \text{A-10}$$

where C_2 is a constant with respect to the space coordinates.

At the water's surface $z = \eta$ and $p = p_a$ is the sea level atmospheric pressure, assumed to be constant with respect to the space coordinates. Evaluating A-10 at the surface gives

$$-\frac{\partial \Psi}{\partial t} \Big|_{z=n} = - \rho g \eta + C_1 - p_a + C_2$$

Since Ψ and η are functions of x and C_1, p_a and C_2 are not, it must be true that

$$C_1 - p_a + C_2 = 0$$

and

$$\frac{\partial \Psi}{\partial t} \Big|_{z=\eta} = g\eta \qquad \text{A-11}$$

We can again use the assumption of reasonably small amplitude waves to advantage by noting that for such waves,

$$\Psi (x, \eta(x)) \approx \Psi (x,0) \qquad \text{A-12}$$

Substituting A-12 into A-11 gives

$$\frac{\partial \psi}{\partial t} = g\eta \qquad \text{A-13}$$

Substituting A-9 into A-12 gives for the dispersion relation

$$\frac{\omega^2}{k} \coth kh = g.$$

At this point we use an assumption that results in considerable simplification of the development to follow. We assume that the water is of sufficient depth (h large enough) so that

$$\coth kh \approx 1$$

and

$$\frac{\omega^2}{k} = g \qquad \text{A-14}$$

Also letting h be very large in A-9 obtains for the velocity potential

$$\psi = -\frac{j\omega a}{k} e^{kz} e^{j(\omega t - kx)} \qquad \text{A-15}$$

Equations A-14 and A-15 describe the behavior of waves where the water is deep enough to attenuate the effect of waves reflected from the ocean floor.

The interaction of the moving sea water having conductivity σ with the constant geomagnetic field $\bar{B}_o$ is described by the magnetohydronamic form of Maxwell's relations

$$\nabla \times \bar{E} = - j\omega\mu\sigma\bar{H} \qquad \text{A-16}$$

$$\nabla \times \bar{H} = \bar{J} \qquad \text{A-17}$$

$$\bar{J} = \sigma (\bar{E} + \bar{v} \times \bar{B}) \qquad \text{A-18}$$

where $\bar{H}$, $\bar{E}$, and $\bar{J}$ are the magnetic field, the electric field and current density respectively. The quantity μ_o is the magnetic permeability of free space. In equation A-17 we have assumed that the displacement currents are negligible and this is quite justified at the frequencies and conductivities involved in this study.

Taking the divergence of equation A-17 we obtain

$$\nabla \cdot \bar{J} = \nabla \cdot (\nabla \times \bar{H}) \equiv 0 \qquad \text{A-19}$$

Taking the divergence of A-18 and using the result in A-19 gives

$$\nabla \cdot \bar{J} = \sigma \nabla \cdot (\bar{E} + \bar{v} \times \bar{B}_o) \equiv 0 \qquad \text{A-20}$$

Here we have assumed that σ is a constant and in this application this appears reasonably valid. Using A-2 for $\bar{v}$ in the term $\bar{v} \times \bar{B}_o$ in A-20 gives

$$\bar{v} \times \bar{B}_o = - \nabla \psi \times \bar{B}_o = - \nabla \times \psi \bar{B}_o \qquad \text{A-21}$$

where the right hand equality results from a vector identity. Solving for $\nabla \cdot \bar{E}$ from A-20 and substituting from A-21 yields

$$\nabla \cdot \bar{E} = - \nabla \cdot (\bar{v} \times \bar{B}_o) = - \nabla \cdot (- \nabla \times \psi \bar{B}_o) \equiv 0$$

$\bar{E}$ is therefore solenoidal and may be expressed as the curl of a vector potential, $\bar{A}^E$. Thus

$$\bar{E} = \nabla \times \bar{A}^E \qquad \text{A-22}$$

Taking the curl of A-16, substituting for $\nabla \times \bar{H}$ from A-17 and for $\bar{E}$ from A-22 and substituting for $\bar{v} \times \bar{B}_o$ from A-21 gives

$$\nabla \times \nabla \times \nabla \times \bar{A}^E + j\omega\mu\sigma \nabla \times \bar{A}^E = j\omega\mu\sigma (\nabla \times \Psi \bar{B}_o) \qquad \text{A-23}$$

Integrating A-23 and using a vector identity yields

$$\nabla \Phi^E + \nabla(\nabla \cdot \bar{A}^E) - \nabla^2 \bar{A}^E + j\omega\mu\sigma\bar{A} = j\omega\mu\Psi \bar{B}_o \sigma$$

where Φ is an arbitrary function of the space coordinates that may be chosen for convenience. To this end we choose

$$\Phi^E = - \nabla \cdot \bar{A}^E$$

to obtain

$$\nabla^2 \bar{A}^E - j\omega\mu\sigma\bar{A}^E = -j\omega\mu\Psi \bar{B}_o\sigma \qquad \text{A-24}$$

Equation A-24 is an inhomogeneous equation for the vector electric potential $\bar{A}^E$ with a source term that involves the motion of the conductive sea water interacting with the geomagnetic field.

Rather than attempt to derive all of the electromagnetic fields from the vector electric potential we will use that potential to derive only a portion of them. In particular we will obtain from the vector electric potential only those fields that can be derived from a solution of A-24 that has only a y component. Reference to A-24 shows that this means that we are seeking only those fields excited by the y component of the geomagnetic field. The fields excited by the x and z components of the geomagnetic field are more conveniently derived from the vector magnetic

potential as will be discussed later. For the present case we assume

$$\bar{A}^E(x,z) = \bar{a}_y A_y(x,z)$$

is a solution to A-24. The electric field may be obtained from $\bar{A}^E$ with the aid of equation A-22. An expression for the magnetic field in terms of $\bar{A}^E$ may be obtained by first solving equation A-16 for $\bar{H}$ and then substituting for $\bar{E}$ from A-22. This yields

$$H = -\frac{1}{j\omega\mu} \nabla \times \nabla \times \bar{A}^E = -\frac{1}{j\omega\mu} (\nabla(\nabla \cdot \bar{A}^E) - \nabla^2 \bar{A}^E) \qquad \text{A-25}$$

where the right hand equality results from an identity for the vector differential operators. Further simplification results if we make use of the fact that $\bar{A}^E$ has only a y component that is independent of y. This implies that

$$\nabla \cdot \bar{A}^E = \frac{\partial A_y^E}{\partial y} = 0$$

so that

$$\bar{H} = \frac{1}{j\omega\mu} \nabla^2 \bar{A}^E \qquad \text{A-26}$$

Substituting for $\nabla^2 \bar{A}^E$ from A-24 gives

$$H = \sigma(\bar{A}^E - \psi B_{oy} \bar{a}_y) \qquad \text{A-27}$$

This simple expression shows that the magnetic field, $\bar{H}$, derived in this manner has only a y component. Since the y component is transverse to the direction of propagation of the ocean waves and to the water motions within the wave we will refer to the $\bar{E}$ and $\bar{H}$ fields derived from $\bar{A}^E$ as Transverse Magnetic (TM) fields.

In order to derive the rest of the electromagnetic fields excited by the ocean wave motions, we note that the magnetic field is solenoidal, as may be verified by taking the divergence of A-16, to write

$$B = \mu_o \bar{H} = D \times \bar{A} \qquad \text{A-28}$$

where $\bar{A}$ is vector magnetic potential. Substituting the expression for $\bar{H}$ obtained from A-28 into A-17 gives

$$\nabla \times \nabla \times \bar{A} = \mu_o \bar{J} \qquad \text{A-29}$$

Substituting for $\bar{J}$ from A-18 and using an identity for the vector differential operations results in the equation

$$\nabla (\nabla \cdot \bar{A}) - \nabla^2 \bar{A} = \mu_o \sigma (\bar{E} + \bar{v} \times \bar{B}). \qquad \text{A-30}$$

We obtain an expression for $\bar{E}$ in terms of $\bar{A}$ by substituting A-28 into A-16 to get

$$\nabla \times \bar{E} = - j\omega \nabla \times \bar{A}$$

Integrating both sides results in

$$\bar{E} = - j\omega A - \nabla \Phi \qquad \text{A-31}$$

where Φ is an arbitrary function of the space coordinates that may be chosen for convenience. We choose

$$\nabla \cdot \bar{A} = - \mu \sigma \Phi \qquad \text{A-32}$$

Substituting this and the expression for $\bar{E}$ from A-31 into A-30 we obtain

$$\nabla^2 \bar{A} - j\omega\mu\sigma\bar{A} = - \mu\sigma\bar{v} \times \bar{B}_o \qquad \text{A-33}$$

Here as before we assume that the vector magnetic potential has a y component only. Thus

$$\bar{A}(x,z) = \bar{a}_y A_y(x,z),$$

where $A_y(x,z)$ is a solution to the y component of equation A-33.

Because A_y is independent of y

$$\nabla \cdot \bar{A}(x,z) = \frac{\partial A_y}{\partial y} = 0$$

According to A-32

$$\Phi = 0$$

so that A-31 becomes

$$\bar{E} = - j\omega\bar{A} \qquad \text{A-34}$$

This equation shows that the electric field derived in this manner has only a y component. Following the same reasoning used to identify the fields derived from the vector electric potential as TM, the fields derived from the vector magnetic potential are termed Transverse Electric (TE).

We summarize the derivations to this point with a review of the equations describing the electromagnetic fields generated by ocean wave motions. In this development the total electromagnetic field is separated into TM and a TE parts that are derived from the y components of the vector potentials $\bar{A}^E$ and $\bar{A}$ respectively. The y components of the potentials are solutions to the y components of equations A-24 and A-33, rewritten here in component form as

$$\nabla^2 A_y^E - j\omega\mu\sigma A_y^E = - j\omega\mu\sigma\Phi B_o \qquad \text{A-35}$$

and

$$\nabla^2 A_y - j\omega\mu\sigma A_y = -\mu\sigma\left(\frac{\partial \psi}{\partial x} B_{oz} - \frac{\partial \psi}{\partial z} B_{ox}\right). \qquad \text{A-36}$$

The velocity potential, ψ, subject to the deep water wave assumption is given by equation A-15 restated here as

$$\psi = -\frac{j\omega a}{k} e^{kz} e^{j(\omega t - kx)} \qquad \text{A-15}$$

The TM electric and magnetic fields are obtained from the vector electric potential with equations A-22 and A-27 respectively. The TE electric and magnetic fields are obtained from equations A-28 and A-34 respectively. We now proceed to obtain solutions to equations A-35 and A-36.

Consider first, solutions to equation A-35. We assume solutions that vary with x and t in the same manner as ψ as indicated in A-15. Thus

$$A_y^E(x,z,t) = A_y^E(z)\, e^{j(\omega t - kx)} \qquad \text{A-37}$$

Substituting A-37 and A-15 into A-35 and performing the derivative with respect to x gives

$$\frac{d^2 A_y^E(z)}{dz^2} - (k^2 + j\omega\mu\sigma) A_y^E(z) = -j\omega\mu\sigma\psi(z) B_{oy} \qquad \text{A-38}$$

where

$$\psi(z) = -\frac{j\omega a}{k} e^{kz} \qquad \text{A-39}$$

The partial second derivative with respect to z implied by the ∇^2 operator in A-35 has been replaced by the total second derivative in A-38 since

$A_y(z)$ varies only with z. Equation A-38 may be written as

$$d^2A_y^E(z) + \zeta^2 A_y^E(z) = f(z) \qquad \text{A-40}$$

where

$$\zeta^2 = -k^2 - j\omega\mu\sigma \qquad \text{A-41}$$

and

$$f(z) = -j\omega\mu\sigma\, B_{oy} \qquad \text{A-42}$$

A particular solution to A-40 may be written as

$$A_{py}^E(z) = \int G(z|z_o)\, f(z_o)\, dz_o \qquad \text{A-43}$$

where the integral is performed over all z_o where $f(z_o)$ is non zero and where

$$G(z|z_o) = \begin{cases} -\frac{1}{j2\zeta}\, e^{-j\zeta(z - z_o)}, & z > z_o \\ -\frac{1}{j2\zeta}\, e^{j\zeta(z - z_o)}, & z < z_o \end{cases} \qquad \text{A-44}$$

Substituting into A-43 from A-42 and A-44 and rearranging terms gives

$$A_{py}^E(z) = \frac{\omega^2\mu\sigma a}{j2\zeta k}\, B_{oy} \left[e^{-j\zeta z} \int_{-\infty}^{z} e^{(k + j\zeta)z_o}\, dz_o + e^{j\zeta z} \int_{z}^{\infty} e^{(k - j\zeta)z_o}\, dz_o \right] \qquad \text{A-45}$$

The integrals in A-45 are easily evaluated and after some algebraic manipulation we obtain for the particular solution

$$A_{py}^E(z) = \frac{j\omega a\, B_{oy}}{k} \left(\frac{k + j\zeta}{j2\zeta}\, e^{j\zeta z} - e^{kz} \right) \qquad \text{A-46}$$

To this solution we add a complementary solution of the homogeneous form of equation A-40,

$$\frac{d^2 A_y^E(z)}{dz^2} + \zeta^2 A_y^E(z) = 0, \qquad \text{A-47}$$

in order to match the electromagnetic boundary conditions. Solutions of A-47 may be written as

$$A_{sy}^E(z) = G\, e^{+j\zeta z} \qquad \text{A-48}$$

where G is an undetermined constant whose value is to be chosen to match the boundary conditions. Consider now the boundary conditions for the TM fields.

In the air above the water's surface ($z > 0$) the electrical conductivity σ is assumed to be zero so that there are no electrical currents and equation A-17 written for the magnetic field intensity in the air (designated by the subscript a) becomes

$$\nabla \times \bar{H}_a = 0 \qquad \text{A-49}$$

Equation A-26 is valid in the air space for $\bar{H}_a$,

$$\bar{H}_a = \frac{1}{j\omega\mu} \nabla^2 \bar{A}_a^E .$$

But, according, to A-24 if $\sigma = 0$

$$\nabla^2 \bar{A}_a^E = 0$$

so we conclude that

$$\bar{H}_a = 0 .$$

This requires that all components of $\bar{H}_a$ including the components tangent to the air sea interface on the air side of the boundary be zero. Because the tangential components of the magnetic field intensity are continuous across a boundary we conclude that on the water side of the interface the components of $\bar{H}$ (as considered here there is only a y component of the TM fields) tangent to the interface are also zero. Using equation A-27 to express the magnetic field we obtain the magnetic field boundary condition in terms of the vector electric potential as

$$A_y^E(o) - \psi(o)\, B_{oy} = 0 \qquad \text{A-50}$$

where the x and t dependence of A_y^E and ψ have been suppressed.

We now add the particular and complementary solutions given by equations A-46 and A-48, substitute the result into A-50 and solve for G to obtain

$$G = -\frac{\omega \underline{a}\,(k + j\zeta)}{2k\zeta}\, B_{oy} \qquad \text{A-51}$$

Using this value for G we write the expression for the vector electric potential from which we derive the total electric vector potential as

$$A_y^E(x,z,t) = -\frac{j\omega \underline{a}}{k} B_{oy}\, e^{kz}\, e^{j(\omega t - kx)} \qquad \text{A-52}$$

Using equations A-22 and A-27 to obtain the electric and magnetic fields gives

$$E_x = j\omega \underline{a}\, B_{oy} e^{kz} \qquad \text{A-53}$$

$$E_z = -\omega a\, B_{oy}\, e^{kz} \qquad \text{A-54}$$

$$H_y = 0 \qquad \text{A-55}$$

TE Fields

In the same fashion as used with the TM fields we assume solutions of A-36 that vary with x and t in the same manner as Ψ as indicated in A-15. Thus

$$A_y(x,z,t) = A_y(z)\, e^{j(\omega t - kx)} \qquad \text{A-56}$$

Substituting A-56 into A-36 and performing the derivative with respect to x gives

$$\frac{d^2 A_y(z)}{dz^2} + \zeta^2 A_y(z) = g(z) \qquad \text{A-57}$$

As before ζ^2 is given by A-41 and

$$g(z) = \mu\sigma k\, \Psi\, (B_{ox} + jB_{oz}) \qquad \text{A-58}$$

A particular solution to A-57 may be written as

$$A_{py}(z) = \int G(z \mid z_o)\, g(z_o)\, dz_o \qquad \text{A-59}$$

where the integral is performed over all z_o for which $g(z_o)$ is non zero. The quantity $G(z \mid z_o)$ is given by A-44.

Substituting into A-59 from A-44 and A-58 and rearranging terms gives

$$A_{py}(z) = \frac{j\omega\mu\sigma a}{2\zeta} (B_{oz} - jB_{ox}) \left[e^{-j\zeta z} \int_{-\infty}^{z} e^{(k+j\zeta)z_o}\, dz_o + e^{j\zeta z} \int_{z}^{o} e^{(k-j\zeta)z_o}\, dz_o \right] \qquad \text{A-60}$$

The integrals in A-60 are easily evaluated and after some manipulation we obtain for the particular solution

$$A_{py}(z) = \frac{a}{} (R_{ox} + jR_{oz}) \left[e^{kz} - \frac{(k+j\zeta)}{j2\zeta} e^{j\zeta z}\right] \qquad \text{A-61}$$

To this solution we add a complementary solution of the homogeneous form of equation A-57

$$\frac{d^2A_y(z)}{dz^2} + \zeta^2 A_y(z) = 0$$

in order to match the electromagnetic boundary conditions. Solutions of the above equation may be written as

$$A_{sy}(z) = F\, e^{j\zeta z}$$

where F is an undetermined constant whose value is to be chosen to match the boundary conditions. Consider now the boundary conditions for the TE fields.

In the air space above the water the y component of the vector magnetic potential satisfies equation A-36 with $\sigma = 0$. Thus

$$\nabla^2 A_{ay} = 0 \qquad \text{A-62}$$

We assume solutions to A-62 that vary with x and t in the same manner as we have assumed for the potentials in the water as expressed by A-56. Substituting into A-62 gives

$$\frac{d^2A_{ay}(z)}{dz^2} - k^2 A_{ay}(z) = 0 \qquad \text{A-63}$$

A solution to A-63 that behaves according to

$$\lim_{z \to \infty} A_{ay}(z) = 0$$

is expressed by

$$A_{ay}(z) = T e^{-kz} \qquad \text{A-64}$$

where T is an undetermined constant.

Both above and below the water's surface the horizontal components of the magnetic and electric fields may be derived from the appropriate vector magnetic potential with the aid of equations A-28 and A-34 respectively. In both the air and the water the vector potential has only a y component so that equations A-28 and A-34 become

$$H(a)x - \frac{1}{\mu_o} \frac{\partial A(a)y(z)}{\partial z} \qquad \text{A-65}$$

and

$$E(a)y - j\omega A(a)y\ (z) \qquad \text{A-66}$$

where the x and t dependence has been supressed. The subscript (a) is intended to mean that equations A-65 and A-66 apply to A_y in the water as well as A_{ay} in the air. In order to evaluate the boundary conditions for the horizontal components of the fields just below the water's surface we first evaluate those fields in the air space just above the surface. Substituting A-64 into A-65 and A-66 and evaluating the result at z = 0 gives

$$H_{ax} = \frac{1}{\mu_o} kT \qquad \text{A-67}$$

and

$$E_{ay} = - j\omega T. \qquad \text{A-68}$$

Because of the continuity of the tangential magnetic and electric fields across an interface we may also write

$$H_x = \frac{1}{\mu_o} kT \qquad \text{A-69}$$

and

$$E_y = - j\omega T \qquad \text{A-70}$$

for the fields on the water side of the interface. Substituting for T in A-69 its value derived from A-70 gives

$$H_x = - \frac{k}{j\omega\mu_o} E_y$$

Substituting for H_x and E_y from A-65 and A-66 and rearranging gives

$$k A_y(o) + \frac{\partial A_y(z)}{\partial z} \Big|_{z=0} = 0 \qquad \text{A-71}$$

as the electromagnetic boundary condition expressed for the vector magnetic potential. If we now add the particular and complementary solutions A-61 and A-63 and substitute the result into A-71 with $z = 0$ we obtain an equation that may be solved for G to give

$$G = \frac{a}{2j\zeta} (B_{ox} + jB_{ox}) \frac{(k - j\zeta)^2}{k + j\zeta} .$$

Using this value for G the total vector magnetic potential written as the sum of the particular and complementary solutions is given by

$$A_y(x,z,t) = \underline{a} (B_{ox} + jB_{oz}) [e^{kz} - \frac{2k}{(k+j\zeta)} e^{j\zeta z}] e^{j(\omega t - kx)} \qquad \text{A-72}$$

Using equations A-28 and A-34 to obtain the electric and magnetic fields gives

$$E_y = - j\omega \underline{a} (B_{ox} + jB_{oz}) \left[e^{kz} - \frac{2k}{k + j\zeta} e^{j\zeta z}\right] \qquad \text{A-73}$$

$$H_x = - \frac{\underline{a}}{\mu} k(B_{ox} + jB_{oz}) \left[e^{kz} - \frac{2j\zeta}{(k + j\zeta)} e^{j\zeta z}\right] \qquad \text{A-74}$$

$$H_z = - j \frac{\underline{a}}{\mu} k(B_{ox} + jB_{oz}) \left[e^{kz} - \frac{2k}{(k + j\zeta)} e^{j\zeta z}\right] \qquad \text{A-75}$$

Equations A-73, A-74 and A-75 give the TE fields generated by the ocean wave motions perpendicular to the geomagnetic field while equations A-53, A-54 and A-55, previously derived give the TM fields.

UNCLASSIFIED

SECURITY CLASSIFICATION OF THIS PAGE (When Data Entered)

REPORT DOCUMENTATION PAGE	READ INSTRUCTIONS BEFORE COMPLETING FORM
1. REPORT NUMBER	2 GOVT ACCESSION NO. / 3. RECIPIENT'S CATALOG NUMBER
4. TITLE (and Subtitle): The Detection of ULF-ELF Emissions from Moving Ships	5. TYPE OF REPORT & PERIOD COVERED: Final Technical Report
	6. PERFORMING ORG. REPORT NUMBER
7. AUTHOR(s): F.X. Bostick, H.W. Smith, J.E. Boehl	8. CONTRACT OR GRANT NUMBER(s): DAAH01 - 74 - C - 0345, ARPA Order - 2605
9. PERFORMING ORGANIZATION NAME AND ADDRESS: Electrical Geophysics Laboratory, The University of Texas at Austin, Austin, TX 78712	10. PROGRAM ELEMENT, PROJECT, TASK AREA & WORK UNIT NUMBERS
11. CONTROLLING OFFICE NAME AND ADDRESS: Defense Advanced Research Projects Agency, 1400 Wilson Blvd., Arlington, VA 22209	12. REPORT DATE: March 1977 13. NUMBER OF PAGES: 104
14. MONITORING AGENCY NAME & ADDRESS (if different from Controlling Office): U.S. Army Missle Command, ATTN: AMSMI-IPWC/Edwards, Redstone Arsenal, AL 35809	15. SECURITY CLASS. (of this report) 15a. DECLASSIFICATION/DOWNGRADING SCHEDULE

16. DISTRIBUTION STATEMENT (of this Report)

Approved for Public Release; distribution unlimited

17. DISTRIBUTION STATEMENT (of the abstract entered in Block 20, if different from Report)

18. SUPPLEMENTARY NOTES

19. KEY WORDS (Continue on reverse side if necessary and identify by block number)

Ocean Wave Noises
Electromagnetic Emissions
Ship Detection
Matched Filters

20. ABSTRACT (Continue on reverse side if necessary and identify by block number)

A series of measurements of the EM emissions from moving merchant ships were made. Analysis of the recorded signals shows that they correspond closely to the fields excited by a horizontal electric dipole source moving with the ship. Also recorded were the levels of the natural EM background. Using these levels the maximum ranges at which a matched filter could extract the ship emission signals are derived. Also considered are the effect of electromagnetic noises generated by ocean surface waves moving the conductive sea

DD FORM 1 JAN 73 1473 EDITION OF 1 NOV 65 IS OBSOLETE

UNCLASSIFIED

SECURITY CLASSIFICATION OF THIS PAGE (When Data Entered)

410133

20.
water in the presence of the geomagnetic field.